

SUBARCSECOND-RESOLUTION RADIO MAPS OF NEARBY SPIRAL GALAXIES

CHAO-WEI TSAI,¹ JEAN L. TURNER,¹ SARA C. BECK,² LUCIAN P. CROSTHWAITE,³ PAUL T. P. HO,^{4,5} AND DAVID S. MEIER^{6,7}

Received 2005 June 11; accepted 2006 August 11

ABSTRACT

We report subarcsecond-resolution Very Large Array imaging of four nearby spiral galaxies: IC 342, Maffei II, NGC 2903, and NGC 6946. In each galaxy, compact radio continuum sources are identified in the central $\sim 15'' \times 15''$ region. These compact sources are responsible for 20%–30% of the total emission from the central kiloparsec of the host galaxies at 2 cm but only $\sim 5\%$ –10% at 6 cm. More than half of the compact sources appear to be H II regions. The H II regions with rising spectra must be fairly dense ($n_i \sim 10^4 \text{ cm}^{-3}$) and are presumably very young. The largest of these H II regions require the excitation of 500–800 O stars within regions only a few parsecs in extent. These clusters approach the sizes expected for globular clusters. Thermal free-free emission from compact sources contributes more significantly at 2 cm, while diffuse synchrotron emission dominates at 6 cm. The radio H II regions are found near the centers of giant molecular clouds in projection and do not have obvious visual counterparts.

Key words: galaxies: individual (IC 342, Maffei II, NGC 2903, NGC 6946) — galaxies: ISM — galaxies: spiral — galaxies: star clusters — H II regions — radio continuum: galaxies

1. INTRODUCTION

Young massive star clusters, potential young globular clusters, have been revealed by ground-based imaging (Arp & Sandage 1985) and *Hubble Space Telescope* (*HST*) observations (see review by Whitmore 2003). These clusters appear to be a few megayears in age, 10^3 – $10^7 M_\odot$ in mass, and 10 pc or smaller in diameter. The youth of these clusters means that, unlike globular clusters, their luminosities are dominated by a population of massive stars. Young, massive star clusters appear to be common (Böker et al. 2002) in the centers of late-type spiral galaxies and may play an important role in galactic nuclear activity. How these large star clusters form and the environments favoring their formation are not understood. The identification of young super star clusters (SSCs) in nearby galaxies gives us the chance to study these clusters in the process of formation.

In nearby starburst galaxies, extremely compact sources with rising spectral indices at centimeter wavelengths have been discovered, which are thought to be “supernebulae” surrounding very young SSCs (Turner et al. 1998, 1999; Kobulnicky & Johnson 1999; Beck et al. 2000; Tarchi et al. 2000; McDonald et al. 2002). These nebulae have the characteristics of dense, compact H II regions in the Galaxy and by analogy are also expected to be very young, ~ 1 Myr or less. However, they are much larger than Galactic compact H II regions, requiring the excitation of hundreds to thousands of young O stars (Turner et al. 1998). These young clusters may be optically obscured by their natal gas and dust clouds (Wood & Churchwell 1989), particularly in molecular gas-rich galactic centers. Free-free emission

from embedded H II regions at radio wavelengths is unaffected by extinction from molecular clouds. Radio continuum emission can be used to search for the youngest, potentially embedded young H II regions in other galaxies.

The goal of this investigation is to identify young SSC candidates in four nearby and well-studied spiral galaxies, IC 342, Maffei II, NGC 2903, and NGC 6946, using subarcsecond radio continuum imaging. The centers of these galaxies are IR-bright (Becklin et al. 1980; Telesco & Harper 1980; Wynn-Williams & Becklin 1985; Ho et al. 1989) and molecular-gas-rich (Rickard et al. 1977; Young & Scoville 1982; Verter 1985). Previous, lower ($\sim 1''$) resolution Very Large Array (VLA) maps have shown that the four galaxies have concentrated regions of star formation in their centers (Turner & Ho 1983, 1994; Wynn-Williams & Becklin 1985). However, the low resolution of these maps, ~ 20 – 70 pc on the galaxy, combines emission from H II regions, supernova remnants (SNRs), and extended nonthermal emission within the beam (Condon 1992). To isolate nebulae around individual star clusters we need subarcsecond resolution.

Subarcsecond imaging with the VLA in its extended configuration maximizes sensitivity to bright and compact radio nebulae over low-brightness disk synchrotron emission. Observing at shorter wavelengths, $\lambda < 2$ cm, also minimizes the contribution of synchrotron emission, which falls with frequency. We present maps of the radio continuum emission at 6 and 2 cm in IC 342, Maffei II, NGC 2903, and NGC 6946 with the A configuration of the VLA. The images have resolutions of $0''.3$ at 6 cm and $0''.1$ at 2 cm, corresponding to size scales of 3 pc (IC 342 and Maffei 2) to 11 pc (NGC 6946) on the galaxies.

2. OBSERVATIONS

Table 1 lists basic properties for the four spiral galaxies. In all four there is prior evidence for compact radio continuum sources (van der Hulst et al. 1981, 1983; Turner & Ho 1983, 1994; Wynn-Williams & Becklin 1985). The radio data were acquired at the NRAO VLA⁸ using the A configuration. Previously unpublished

¹ Department of Physics and Astronomy, University of California at Los Angeles, Los Angeles, CA 90095-1547; cwtsai@astro.ucla.edu, turner@astro.ucla.edu.

² Department of Physics and Astronomy, Tel Aviv University, Ramat Aviv, Israel; sara@wise1.tau.ac.il.

³ Northrop Grumman, San Diego, CA 92123; lpcrosthwaite@cox.net.

⁴ Harvard-Smithsonian Center for Astrophysics, Cambridge, MA 02138; ho@cfa.harvard.edu.

⁵ Institute of Astronomy and Astrophysics, Academia Sinica, P.O. Box 23-141, Taipei 106, Taiwan.

⁶ Jansky Fellow; National Radio Astronomy Observatory, P.O. Box O, Socorro, NM 87801; dmeier@nrao.edu.

⁷ Department of Astronomy, University of Illinois, Urbana, IL 61801.

⁸ The National Radio Astronomy Observatory is a facility of the National Science Foundation operated under cooperative agreement by Associated Universities, Inc.

TABLE 1
PROPERTIES OF THE SAMPLE GALAXIES

Galaxy	Hubble Type	D^a (Mpc)	S_6^b (mJy)	S_2^b (mJy)	$S_6^{\text{map}c}$ (mJy)	$S_2^{\text{map}c}$ (mJy)	L_{IRAS}^d ($10^9 L_\odot$)	$M(H_2)^e$ ($10^8 M_\odot$)
IC 342	SAB(rs)cd	3.3	82	38	15	7	3.0	6.8
Maffei II	SAB(rs)bc	5.0	107	46	16	13	12.3	3.7
NGC 2903	SB(s)d	8.9	35	12	5	6	9.4	4.5
NGC 6946	SAB(rs)cd	5.9	39	23	17	8	7.2	4.9

^a Reference papers for distance: IC 342, Saha et al. (2002); Maffei II, Hurt et al. (1993a); NGC 2903, Drozdovsky & Karachentsev (2000); NGC 6946, Karachentsev et al. (2000).

^b Total radio continuum fluxes in VLA low-resolution maps using the B configuration at 6 cm and the C configuration at 2 cm for IC 342, NGC 6946 (Turner & Ho 1983), and Maffei II (Turner & Ho 1994) and the C configuration at 6 cm for NGC 2903 (Wynn-Williams & Becklin 1985).

^c Total fluxes in naturally weighted $0''3$ maps (this paper).

^d L_{IRAS} (IR luminosity) calculated using the prescription from Sanders & Mirabel (1996). *IRAS* data are from point-source flux densities listed in the *IRAS* Faint Source Catalog, version 2.0 (Moshir et al. 1990). *IRAS* fluxes of Maffei II are from Chini et al. (1986).

^e Molecular mass calculated using ^{12}CO data (Sage et al. 1990) with distance correction.

TABLE 2
VLA DATA

Band ^a	Obs. Date	On Source (s)	Config.	Flux Calib.	Phase Calib.	Prog. ID	
IC 342							
C.....	1996 Nov 23	5290	A	3C 48	0224+671	AW419	
	1988 Nov 20	4040	A	3C 48 and 3C 147	0224+671	AT98 ^b	
	1981 Jul 11	6260	A	3C 286	0212+735	AT21	
U.....	1999 Aug 23	4310	A	3C 286	0228+673	AT227 ^b	
	1995 Dec 8	4550	B	3C 48	0224+671	AW419	
	1981 Nov 14	6020	C	3C 286	0224+671	AT21	
Maffei II							
C.....	1989 Aug 26	6860	BC	3C 138 and 3C 48	0224+671	AH353	
	1988 Nov 20	4020	A	3C 48 and 3C 147	0224+671	AT98 ^b	
	1982 Sep 5	2970	B	3C 286	0224+671	AT21	
	1982 Sep 4	5570	B	3C 286	0224+671	AT21	
U.....	1983 Oct 12	2330	A	3C 48 and 3C 138	0224+671	AH141 ^b	
	1983 Apr 18	4090	C	3C 286	0224+671	AT25	
	1983 Apr 18	1170	C	3C 286	0224+671	AT25	
NGC 2903							
C.....	1997 Jan 11	4340	A	3C 286	0851+202	AW419	
	1996 Nov 26	4320	A	3C 286	0851+202	AW419	
	1988 Nov 18	3470	A	3C 286	0851+202	AT98 ^b	
	1988 Feb 1	870	B	3C 286	0953+254	AS314	
	1986 Aug 16	870	B	3C 48	0953+254	AD176	
	1985 Apr 26	5530	B	3C 286	0851+202	AB324	
	1982 Oct 24	8550	B	3C 286	0851+202	AT21	
	U.....	1999 Aug 23	4280	A	3C 286	0854+201	AT227 ^b
		1996 Apr 14	1500	C	3C 286 and 3C 147	1004+141	AQ11
		1996 Jan 5	3840	B	3C 48	0851+202	AW419
1995 Dec 27		1800	B	3C 286	0851+202	AW419	
1986 Dec 8		17100	C	3C 286	0851+202	AB324	
C.....	1985 Sep 18	9480	C	3C 286	0851+202	AB324	
	1983 Apr 18	2210	C	3C 286	0851+202	AT25	
	1983 Apr 17	2900	C	3C 286	0851+202	AT25	
	NGC 6946						
C.....	1999 Jun 17	3680	AD	3C 48	2021+614	AS568	
	1996 Nov 23	4730	A	3C 48	2021+614	AW419	
	1994 Apr 10	6340	A	3C 286	2021+614	AS525	
	1988 Nov 20	4010	A	3C 48 and 3C 147	2021+614	AT98 ^b	
U.....	1995 Dec 8	4580	B	3C 48	2021+614	AW419	
	1983 Oct 12	2600	A	3C 48 and 3C 138	2021+614	AH141 ^b	
	1981 Nov 14	6020	C	3C 286	2021+614	AT21	

^a VLA C band, 6 cm; U band, 2 cm.

^b Unpublished data from observations executed by the authors.

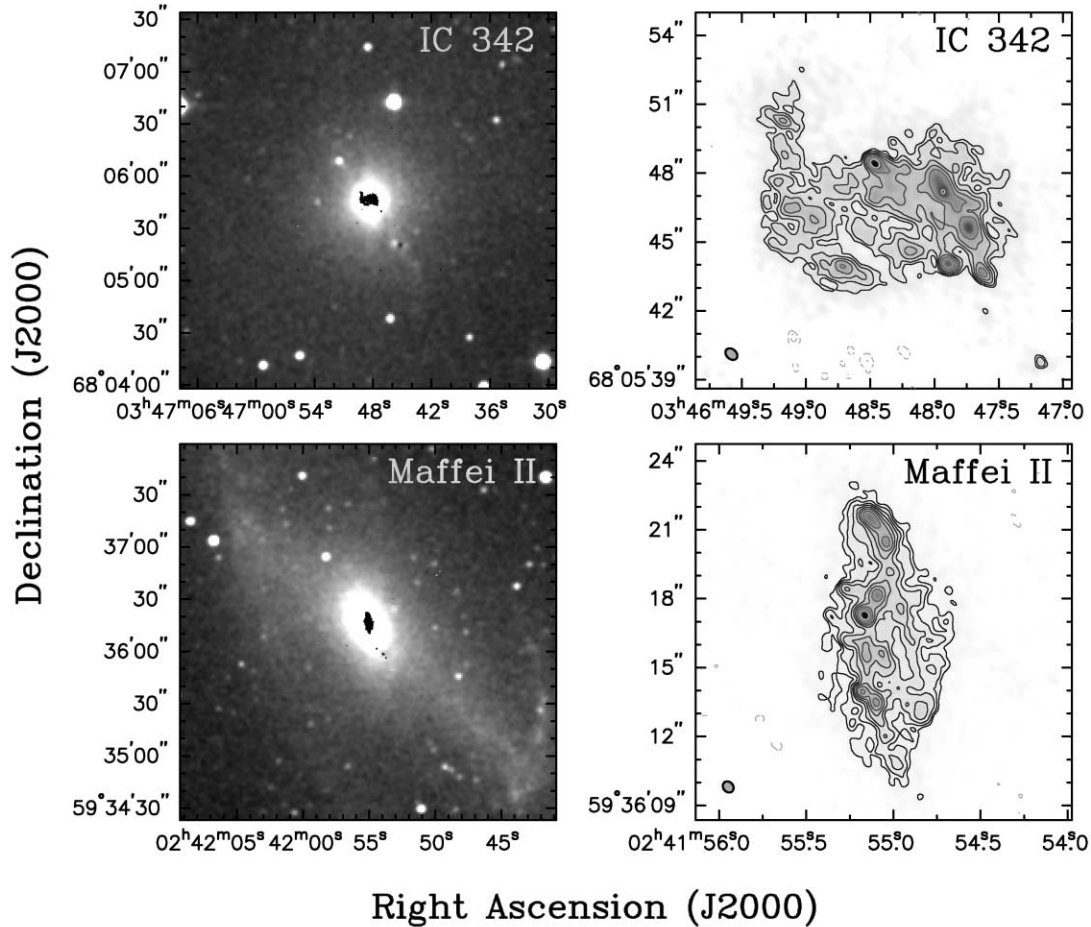


FIG. 1.—2MASS K -band images and VLA 6 cm radio continuum maps of our four sample galaxies. On the left are $3\frac{1}{6} \times 3\frac{1}{6}$ visible images from a 2MASS K band overlaid with 6 cm radio emission from the central region. On the right are 6 cm maps with a $16'' \times 16''$ field of view, contoured at half-integral powers of $2 \times 0.14 \text{ mJy beam}^{-1}$ ($\sim 4 \sigma$). Peak flux densities are 1.49, 3.13, 0.37, and $2.74 \text{ mJy beam}^{-1}$ for IC 342, Maffei II, NGC 2903, and NGC 6946, respectively. Beams are $0\text{''}.3$ in size.

6 cm continuum data were obtained on 1988 November 18 and 20 (program AT98), and 2 cm data were obtained on 1983 October 12 (program ID AH141) and 1999 August 23 (program AT227). The 2 cm observations in 1999 August were made using fast switching, with cycle times of 2 minutes. On-source integration times were ~ 1 hr at both wavelengths. Data calibration was done using AIPS, following high-frequency reduction procedures for the 2 cm calibration. The sources 3C 48, 3C 138, 3C 147, and 3C 286 were used as flux calibrators. The uncertainty in the absolute flux scale was $\leq 5\%$. Observational parameters are shown in Table 2.

To enhance the sensitivity, we combined our VLA A configuration data with previously published VLA archival data listed in Table 2. Data sets of A, B, or C configurations with time on-source > 10 minutes and phase center within $18''$ (1/10 of the VLA primary beam at 2 cm) from the centers of our measurements were used. Observations with B1950.0 equinox coordinates were precessed to J2000.0 coordinates; the uncertainty for this conversion is ~ 20 mas. The uncertainty in the absolute position is determined by the B1950.0 calibrator positions, which are good to 50 mas.

Spectral index measurements were done with a separate set of maps with matching (u, v) -coverages at 6 and 2 cm, which include matched shortest baselines of the A configuration at 2 cm and longest baselines of the A configuration at 6 cm. The largest angular scales sampled by the images are $\sim 6''$. Fluxes and peak fluxes are therefore lower limits to the total flux if extended emis-

sion is present. The images were then convolved to the same beam size to have matching maximum baseline lengths. Final rms noise levels in blank regions of the maps are $\sim 0.05, 0.04, 0.03,$ and $0.03 \text{ mJy beam}^{-1}$ for IC 342, Maffei 2, NGC 2903, and NGC 6946, respectively, at 6 cm and $\sim 0.09, 0.1, 0.05,$ and $0.14 \text{ mJy beam}^{-1}$ at 2 cm.

While it is impossible to precisely match (u, v) -coverages or to quantify the differences without prior knowledge of the extended source structure, the (u, v) -plane is well sampled, and we estimate that differences between the maps caused by the differences in undersampled extended emission ($> 10''$) must be less than the total resolved-out flux divided by this area, which comes to less than our noise level. Since the compact sources we identify are all much less than $10''$ in extent, the effects on our fluxes with differences in (u, v) -coverages will be undetectable.

Interferometer maps are high-pass filtered images, and it is difficult to assign uncertainties without knowing the extended structure, which is not known a priori. Point sources and sources that are well sampled by the (u, v) -coverage will have uncertainties that are described well by the rms noise. Most of our sources fall into this category. We have fitted sizes to the extended sources to better estimate flux uncertainties for these sources.

Although the differences between 6 and 2 cm spatial sampling may not affect compact source fluxes, we stress that there is extended unresolved flux in these maps. One generally compares single-dish fluxes to mapped VLA fluxes to estimate how much extended emission is resolved out of the VLA maps. In this case,

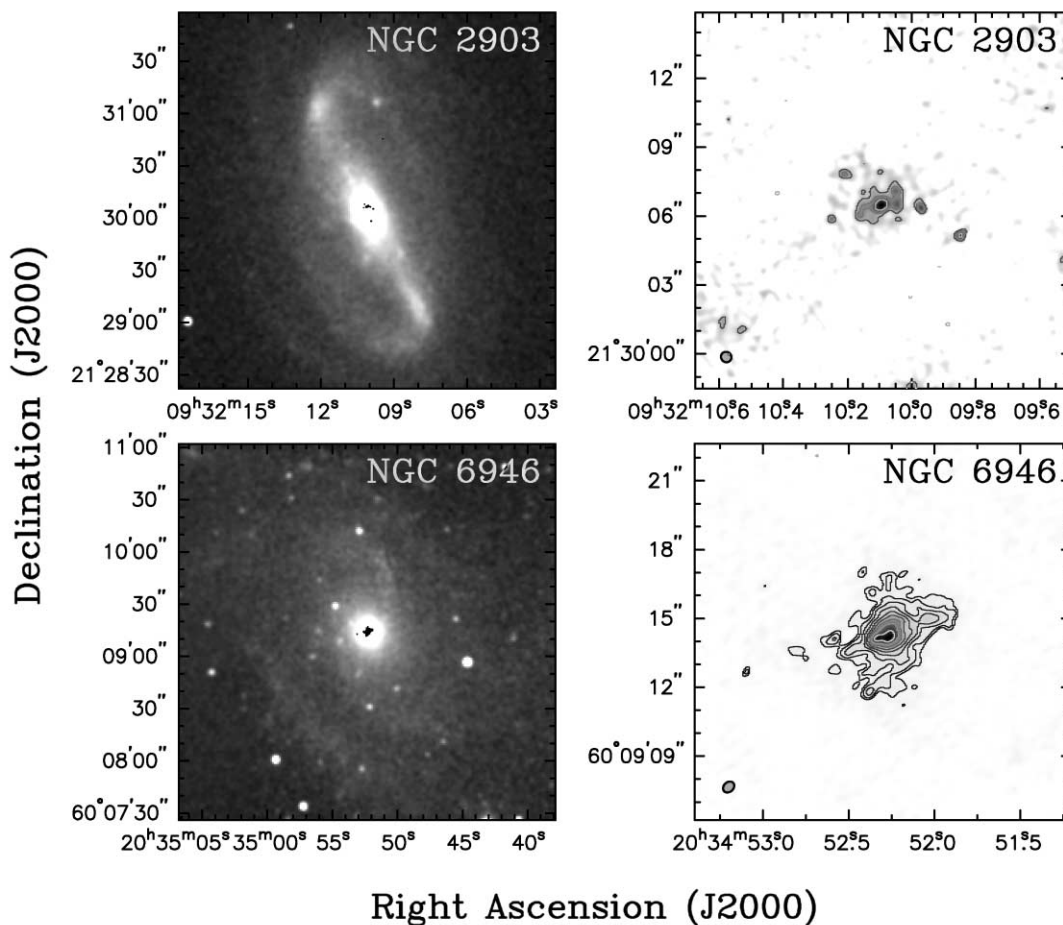


FIG. 1.—Continued

the disparity between single-dish beams, typically a few arcminutes in size, and our subarcsecond beams makes this comparison difficult. We therefore compare our compact-source fluxes to lower resolution VLA maps in the B and C configurations (shown in Table 1) to see how much flux is resolved out; these lower resolution maps are sensitive to structures up to $45''$ across at 6 and 2 cm, except in the case of NGC 2903, in which the C configuration flux at 6 cm (sensitive to structure $\geq 120''$ in size) has been quoted. The total mapped fluxes indicate that our maps recover 15%–45% of the 6 cm flux in the lower resolution observations and 20%–45% of the 2 cm flux in both compact and extended components.

3. THE RADIO CONTINUUM IMAGES AND THE COMPACT RADIO SOURCES

The 6 cm radio continuum maps and K -band ($2.2 \mu\text{m}$) images of the four galaxies are shown in Figure 1. The naturally weighted radio contours are overlaid on Two Micron All Sky Survey (2MASS) K -band images on the left. In each of the galaxies the nucleus is a strong $2 \mu\text{m}$ source and the 6 cm continuum is strongest at the center. We see emission from the central ~ 150 pc except in the case of Maffei II, in which the emission extends over a distance of ~ 350 pc.

The 6 cm maps in the right panels of Figure 1, contoured at the same 4σ levels as in the overlay in the left panels, are close-ups of the radio emission region within the central $16''$ – $26''$. In each source there are strong compact sources embedded in extended emission. The western part of the extended emission in IC 342 contains five sources aligned from northwest to south-

east (named A–E in Table 3), while the eastern part has fewer sources and their emission is also significantly weaker. Ten sources are identified in Maffei II, spread out over $10''$ (~ 240 pc) north-south on the eastern edge of the extended emission. The 6 cm continuum emission in NGC 2903 and NGC 6949 is confined to single central sources surrounded by extended emission. The diffuse emission is “patchy” because the large-scale extended emission has been resolved out by the high resolution. We discuss features in the individual galaxies in subsequent sections. Peak flux densities at 6 cm are 1.2, 2.6, 0.4, and 1.9 mJy beam^{-1} for IC 342, Maffei II, NGC 2903, and NGC 6946, respectively.

The radio maps are overlaid on HST V -band and $H\alpha$ images in Figures 2–5. For convenience in comparing to the 2 cm, the 6 cm maps in Figures 2–5 were restricted to the same (u, v) -coverage (~ 30 – 600 $k\lambda$) and convolved to the same beam size. The radio and HST images have similar resolutions. The uncertainty in the registration of the images is $\sim 1''$, limited by the astrometry of the HST images. In IC 342, Maffei II, and NGC 2903 the radio sources tend to lie in regions of apparent dust obscuration. In NGC 6946 the extended central radio continuum source nearly aligns with a bright optical source at the center. The uncertainty in registration does not allow us to determine how precisely they align.

In Table 3 we list compact sources detected in the central $15''$ radius of each galaxy and their fluxes at 6 and 2 cm, with proper (u, v) -restrictions described in § 2. The sources meet at least one of the following criteria: (1) 5σ detection at the peak intensity at one wavelength and (2) 4σ emission detection in both wave bands. The sources are named alphabetically following

TABLE 3
COMPACT CONTINUUM SOURCE OBSERVED QUANTITIES

Source	α (J2000.0)	δ (J2000.0)	$S_{6\text{ cm}}^{\text{Peak a,b}}$ (mJy beam $^{-1}$)	$S_{6\text{ cm}}^{\text{b,c}}$ (mJy)	$S_{2\text{ cm}}^{\text{Peak a,b}}$ (mJy beam $^{-1}$)	$S_{2\text{ cm}}^{\text{b,c}}$ (mJy)	Size ^d (arcsec)	P.A. (deg)
IC 342								
A.....	03 46 48.46	68 05 48.4	1.4	1.5 \pm 0.2	0.6	0.9 \pm 0.3	0.2 \times 0.1	40
B.....	03 46 47.88	68 05 44.1	0.8	0.8 \pm 0.2	<0.3 ^e	0.4 \pm 0.3	0.3 \times 0.1	120
C.....	03 46 47.73	68 05 45.7	0.8	1.3 \pm 0.3	1.0	2.2 \pm 0.5	0.4 \times 0.3	20
D.....	03 46 47.93	68 05 47.3	0.8	1.5 \pm 0.4	<0.3 ^e	<0.3	0.6 \times 0.4	10
E.....	03 46 47.61	68 05 43.7	0.5	0.7 \pm 0.3	0.7	0.7 \pm 0.5	0.4 \times 0.3	40
F.....	03 46 47.98	68 05 47.8	0.5	0.6 \pm 0.3	<0.3 ^e	<0.3	0.4 \times 0.3	70
G.....	03 46 48.69	68 05 44.0	0.5	0.6 \pm 0.3	0.5	0.5 \pm 0.5	0.5 \times 0.3	100
H.....	03 46 49.18	68 05 50.3	0.4	0.5 \pm 0.3	<0.3 ^e	<0.3	0.4 \times 0.3	140
I.....	03 46 47.86	68 05 45.5	<0.2 ^e	<0.2	0.7	0.7 \pm 0.5	0.4 \times 0.3	120
J.....	03 46 48.50	68 05 47.2	<0.2 ^e	<0.2	0.7	0.7 \pm 0.5	0.8 \times 0.2	10
K.....	03 46 48.17	68 05 48.5	<0.2 ^e	<0.2	0.7	0.7 \pm 0.5	0.4 \times 0.3	150
L.....	03 46 48.99	68 05 46.4	<0.2 ^e	<0.2	0.7	0.7 \pm 0.4	0.4 \times 0.2	70
Maffei II								
A.....	02 41 55.16	59 36 17.3	2.6	3.1 \pm 0.2	2.1	2.7 \pm 0.5	0.3 \times 0.2	60
B.....	02 41 55.14	59 36 21.5	1.1	1.1 \pm 0.2	<0.3 ^e	<0.3	0.4 \times 0.3	60
C.....	02 41 55.10	59 36 21.2	1.0	1.6 \pm 0.2	1.7	2.2 \pm 0.6	0.4 \times 0.3	70
D.....	02 41 55.09	59 36 18.1	1.0	1.5 \pm 0.3	1.3	1.8 \pm 0.7	0.5 \times 0.4	150
E.....	02 41 55.17	59 36 13.9	0.8	0.8 \pm 0.2	1.2	1.3 \pm 0.5	0.3 \times 0.2	160
F.....	02 41 55.04	59 36 20.5	0.8	1.6 \pm 0.2	1.0	1.0 \pm 0.4	0.2 \times 0.1	70
G.....	02 41 55.10	59 36 13.5	0.8	1.2 \pm 0.2	0.8	1.5 \pm 0.4	0.5 \times 0.1	0
H.....	02 41 55.16	59 36 15.5	0.7	1.0 \pm 0.3	0.8	1.4 \pm 0.7	0.5 \times 0.4	10
I.....	02 41 55.07	59 36 15.6	0.6	0.9 \pm 0.3	0.8	0.8 \pm 0.8	0.6 \times 0.4	40
J.....	02 41 55.15	59 36 15.9	0.6	0.7 \pm 0.3	<0.3 ^e	<0.3	0.5 \times 0.4	80
NGC 2903								
A.....	09 32 09.85	21 30 05.2	0.3	0.4 \pm 0.1	0.2	0.4 \pm 0.2	0.4 \times 0.2	150
B.....	09 32 10.10	21 30 06.5	0.3	0.5 \pm 0.2	0.4	1.2 \pm 0.4	0.6 \times 0.4	120
C.....	09 32 09.93	21 29 58.1	0.3	0.4 \pm 0.2	0.3	0.3 \pm 0.3	0.4 \times 0.3	100
D.....	09 32 09.97	21 30 06.3	0.2	0.2 \pm 0.1	<0.1 ^e	<0.1	0.2 \times 0.2	60
E.....	09 32 10.21	21 30 07.9	0.2	0.2 \pm 0.1	0.2	0.4 \pm 0.2	0.4 \times 0.2	140
F.....	09 32 09.76	21 30 01.3	<0.1 ^e	<0.1	0.3	0.4 \pm 0.3	0.5 \times 0.4	90
G.....	09 32 10.00	21 30 07.5	<0.1 ^e	<0.1	0.2	0.3 \pm 0.2	0.4 \times 0.2	50
NGC 6946								
A.....	20 34 52.34	60 09 14.2	1.5	...	1.1	...	Confused	...
B.....	20 34 52.28	60 09 14.2	1.4	...	1.5	...	Confused	...
C.....	20 34 52.28	60 09 14.5	1.1	...	0.7 ^f	...	Confused	...
D.....	20 34 52.25	60 09 14.7	1.0 ^f	...	1.0	...	Confused	...
E.....	20 34 52.03	60 09 15.0	0.3	0.5 \pm 0.2	0.5	0.5 \pm 0.5	0.5 \times 0.3	120
F.....	20 34 52.39	60 09 11.9	0.2	0.3 \pm 0.1	<0.4 ^e	<0.4	0.3 \times 0.2	70
G.....	20 34 52.15	60 09 14.5	0.2	0.3 \pm 0.3	<0.4 ^e	<0.4	0.9 \times 0.5	130
H.....	20 34 52.50	60 09 13.6	0.1	0.3 \pm 0.1	<0.4 ^e	<0.4	0.4 \times 0.2	140
I.....	20 34 52.23	60 09 14.2	0.4 ^f	...	1.3	...	Confused	...

NOTE.—Units of right ascension are hours, minutes, and seconds, and units of declination are degrees, arcminutes, and arcseconds.

^a Here $S_{6\text{ cm}}^{\text{Peak}}$ and $S_{2\text{ cm}}^{\text{Peak}}$ are the peak flux density (intensity) of 6 and 2 cm continuum, respectively, with beams $0''.45 \times 0''.42$, P.A. = 46° for IC 342; $0''.43 \times 0''.42$, P.A. = 40° for Maffei II; $0''.43 \times 0''.42$, P.A. = 82° for NGC 2903; and $0''.42 \times 0''.38$, P.A. = -79° for NGC 6949. The rms noise levels at 6 cm are 0.05, 0.04, 0.03, and 0.03 mJy beam $^{-1}$ for IC 342, Maffei II, NGC 2903, and NGC 6946, respectively, and those at 2 cm are 0.09, 0.11, 0.05, and 0.14 mJy beam $^{-1}$, respectively.

^b Flux densities are measured in the (u , v)-restricted map. The uncertainties quoted here are 3σ . See text for details.

^c Here $S_{6\text{ cm}}$ and $S_{2\text{ cm}}$ are the total integrated fluxes at 6 and 2 cm, respectively. Quoted uncertainties in the fluxes are derived from the rms and measured source size; intensities are more accurate for extended sources. The systematic error of flux is expected to be $\lesssim 5\%$.

^d Single-Gaussian fitting uncertainty is $\lesssim 30\%$, using the AIPS task *imfit*.

^e 3σ upper limit.

^f Peak flux density is the averaged flux density over a beam area.

radio convention in order of their peak flux densities at 6 cm. Positions and deconvolved sizes of sources were obtained from the 2 cm data fit assuming a single-Gaussian source using the *imfit* task in AIPS. For sources absent at 2 cm, Gaussians were fitted to the 6 cm maps. The uncertainty in size is $\lesssim 30\%$ of the

beam. The total integrated flux densities were measured using the AIPS task *iring*. The upper limits quoted for nondetections are 3σ . The systematic error of flux is expected to be $\lesssim 5\%$, related to the uncertainties in the absolute flux calibration fluxes. We separated this uncertainty from the signal-to-noise ratio.

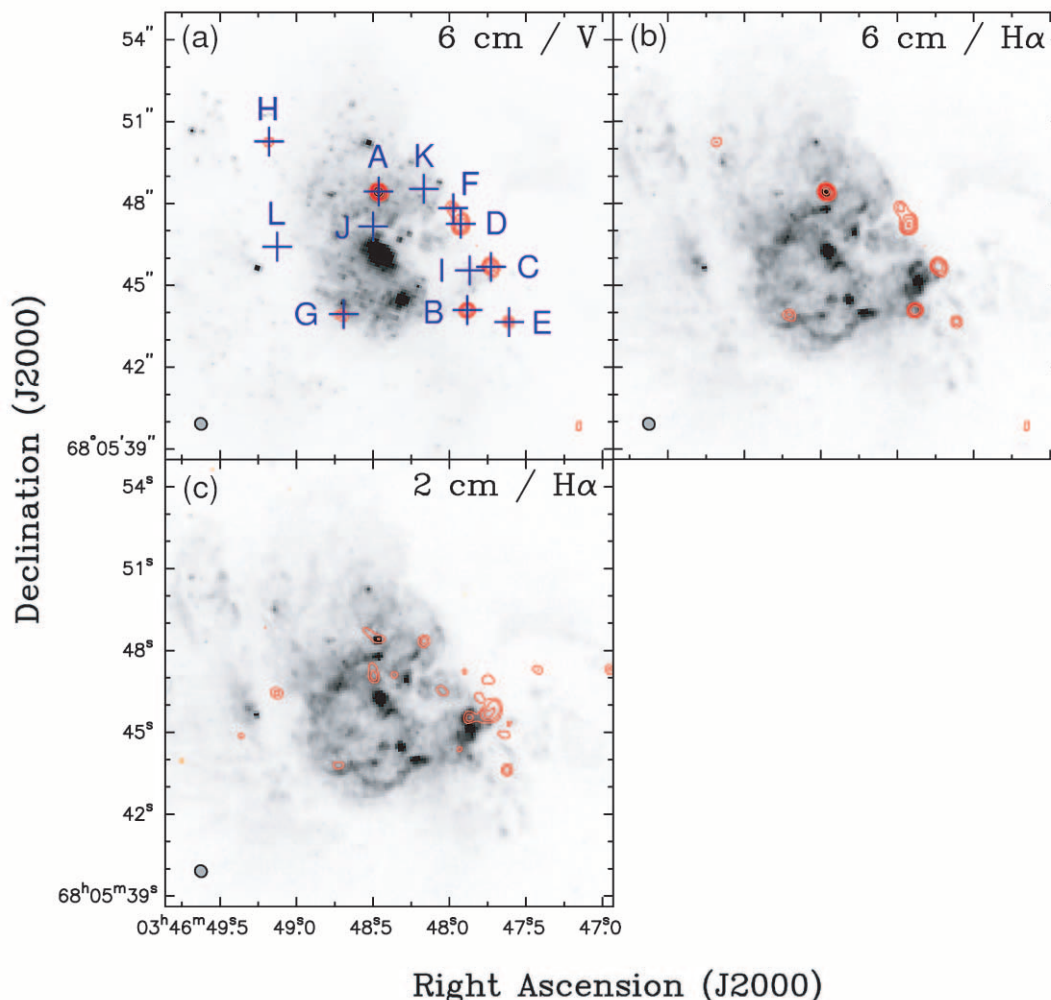


FIG. 2.—Close-ups of the central region of IC 342. (a) 6 cm contours overlaid on a WFPC2 V -band (F555W) image. (b) 6 cm contours overlaid on a WFPC2 $H\alpha$ (F656N) image. (c) 2 cm contours overlaid on a WFPC2 $H\alpha$ (F656N) image. The beam size of each map has been matched to $0''.45 \times 0''.42$, P.A. = 46° . Contours are half-integral powers of $\pm 2 \times 0.30$ and 0.43 mJy beam $^{-1}$ for 6 and 2 cm, respectively. Uncertainty in the registration of the VLA and *HST* maps is $\sim 1''$.

In Table 4 we list the properties of each compact radio source. The spectral index is defined as $S_\nu \propto \nu^\alpha$. The uncertainties of α_{6-2} , the spectral index between the 2 and 6 cm wavelengths, are derived with $\sqrt{2}$ σ variances of flux densities in both wave bands; uncertainties are typically ± 0.2 – 0.3 . For sources A–D and I in the extended emission complex of NGC 6946, we derive α from their intensities, which are well determined, rather than their fluxes, which are more uncertain. Based on the values of α_{6-2} (discussed in the next section), we classified sources as optically thick $H II$ regions ($H II$, thick), optically thin $H II$ regions ($H II$, thin), SNRs, or radio supernovae (RSNe). Source types are listed in columns (3) and (4) in Table 4. For the cases identified as $H II$ regions, N_{Lyc} in column (5) is the Lyman continuum rate derived from the flux density at 2 cm on the assumption of optically thin emission and electron temperature in the $H II$ region, $T_e \sim 10,000$ K. If the emission is optically thick, this value will be a lower limit to the true N_{Lyc} value. The electron temperatures of $H II$ regions tend to be cooler toward the high-metallicity centers of spiral galaxies (Pagel et al. 1979; Sedwick & Aller 1981). The values of N_{Lyc} will be $\sim 15\%$ lower than listed if $T_e = 6000$ K rather than the adopted 10^4 K. The N_{O7} value is the number of standard O7 stars needed to generate N_{Lyc} . We also assume ionization-bonded nebulae; if UV photons escape the $H II$ region, our OB luminosities will be underestimates of the true Lyman continuum rates.

4. DISCUSSION

4.1. Identification of Luminous Compact $H II$ Regions from their Radio Spectra

The radio images reveal a population of bright compact radio sources in the centers of IC 342, Maffei II, NGC 6946, and NGC 2903. The sources are comparable in extent to the $0''.3$ beam, or ~ 5 – 10 pc in diameter. What are these sources?

The centimeter-wave continuum emission from nearby normal galaxies is a mixture of synchrotron emission from SNRs and disk cosmic rays and thermal bremsstrahlung emission from $H II$ regions. The spectral index α is an indicator of the emission mechanism: optically thin free-free emission has $\alpha \sim -0.1$, while optically thin nonthermal emission by synchrotron radiation will have steeper negative spectral indices. Galactic SNRs have $\alpha_{nt} \sim -0.6$ to -0.2 , with the majority in the range -0.5 to -0.4 (Green 1984; Mills et al. 1984; Weiler et al. 1986). Steeper $\alpha_{6-2} < -1.0$ are characteristic of short-lived RSNe (Weiler et al. 1986) and extended synchrotron disk emission.

$H II$ regions are optically thick at wavelengths longer than a turnover frequency that depends on the electron temperature and emission measure, $EM = \int n_e^2 dl$. At long wavelengths, $H II$ regions are bright and their fluxes rise with frequency until the turnover frequency. The higher the emission measure, the higher the turnover frequency. Spectra of diffuse or “classical”

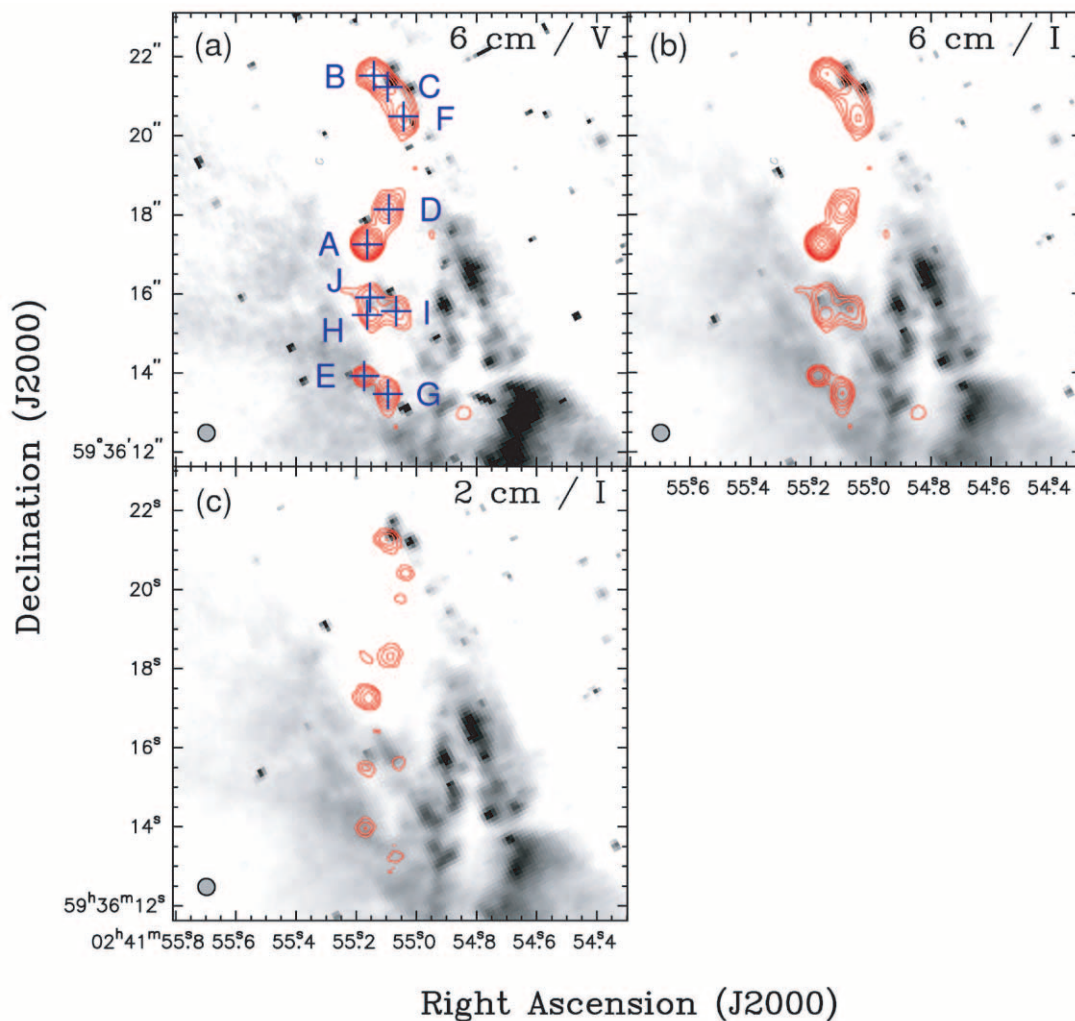


FIG. 3.— Close-ups of the central region in Maffei II. (a) 6 cm contours overlaid on a WFPC2 *V*-band (F606W) image. (b) 6 cm contours overlaid on a WFPC2 *I*-band (F814W) image. (c) 2 cm contours overlaid on a WFPC2 *I*-band (F814W) image. The beam size of each map has been matched to $0''.43 \times 0''.42$, P.A. = 40° . Contours are at half-integral powers of $\pm 2 \times 0.21$ and 0.60 mJy beam $^{-1}$ for the 6 and 2 cm maps, respectively. Uncertainty in the registration of the VLA and *HST* maps is $\sim 1''$.

($EM \leq 10^4$ cm $^{-6}$ pc) H II regions that appear in visible wavelengths typically turn over at meter wavelengths and are optically thin at centimeter wavelengths. A centimeter-wave turnover frequency is characteristic of compact or ultracompact H II regions (Mezger & Henderson 1967), which have $EM \geq 10^8$ – 10^9 cm $^{-6}$ pc.

Beyond the Local Group, ultracompact H II regions typical of those in our Galactic disk, excited by individual O stars or small clusters, are small in size (Habing & Israel 1979) and are thus too faint to be seen (Turner & Ho 1994). The compact component (Mezger et al. 1967) of the luminous Galactic H II region W49 would fail to meet our detection criteria in our closest galaxy (IC 342), as would the radio source (de Pree et al. 1999) of NGC 3606. However, if the clusters are somewhat larger, with at least 200 O stars surrounded by an ionization-bounded volume of gas, even dense, compact H II regions with $EM \geq 10^8$ – 10^9 cm $^{-6}$ pc can be detected in external galaxies (Turner et al. 1998). Even for the largest clusters ($N_{O7} = 10^4$), dense, compact H II regions will still be small, less than 2–3 pc in size. Since large numbers of massive stars can also be accompanied by supernovae, thermal free-free emission from these H II regions can be mixed with nonthermal emission within a single beam if the resolution is low (Turner et al. 1998, 2000). Confusion is minimized if the

resolution is high and the galaxy is nearby so that the beam closely matches the size of a single H II region. Subarcsecond imaging maximizes our sensitivity to these sources.

More than half of the 38 identified compact sources of Table 4 appear to be H II regions. A significant fraction may have rising spectra, indicating that they are at least partly optically thick at 6 cm. Given the likely presence of nonthermal synchrotron emission in the vicinity of these star-forming regions, the spectral indices could systematically be even higher than we measure here due to spectral confusion (Turner et al. 2000). Rising centimeter-wave spectra imply that the rms electron densities are $\sim 10^3$ – 10^4 cm $^{-3}$. That a large percentage of our sources are ultracompact H II regions might be expected from the subarcsecond resolution, which picks out these high-brightness regions. There may be lower density, extended, and less bright H II regions that are below the brightness limit of these maps.

4.2. Compact Nebulae as Young Star Formation Tracers

4.2.1. Properties of the Compact H II Regions

The sizes of the compact H II regions listed in Table 3 are obtained from deconvolution of the beam from the observed

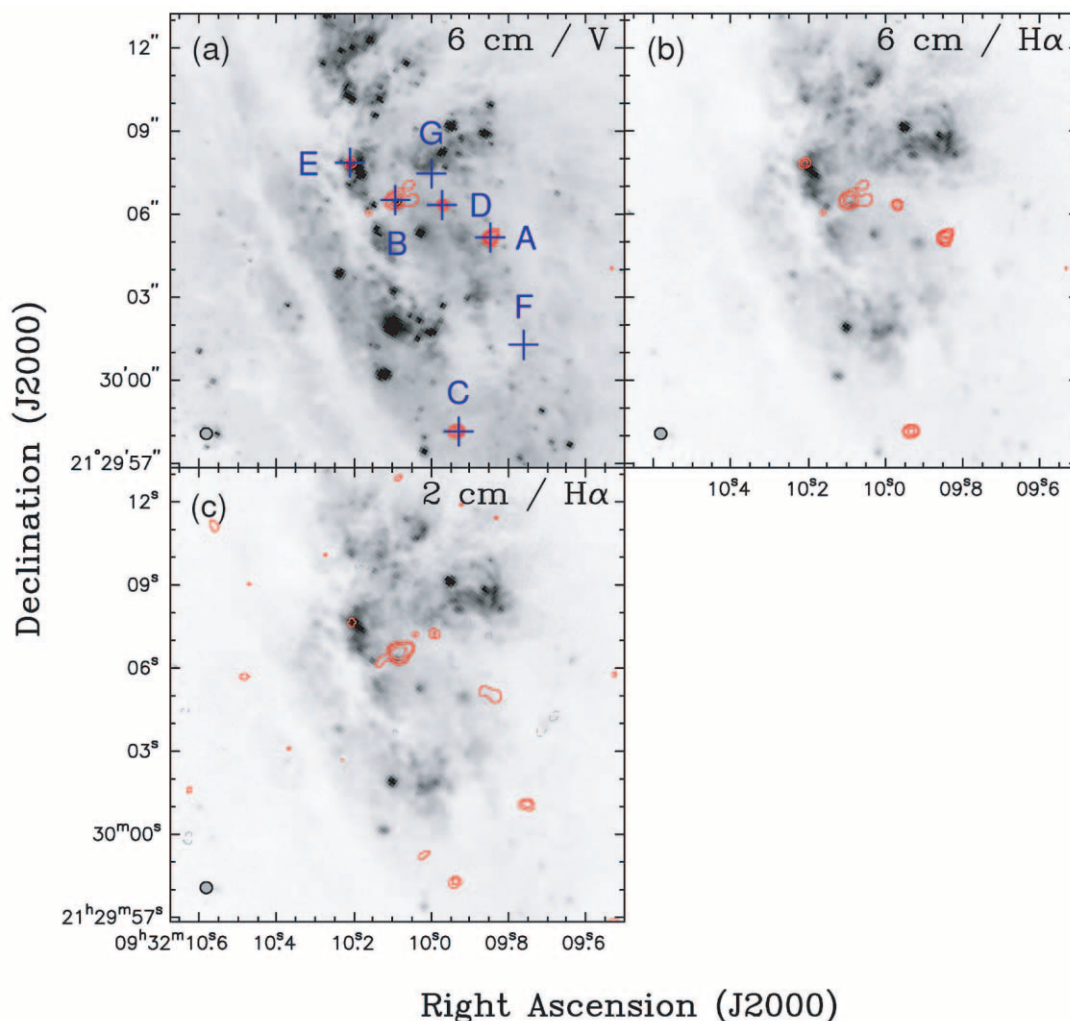


FIG. 4.—Close-ups of the central region in NGC 2903. (a) 6 cm contours overlaid on a WFPC2 *V*-band (F555W) image. (b) 6 cm contours overlaid on a WFPC2 $H\alpha$ (F656N) image. (c) 2 cm contours overlaid on a WFPC2 $H\alpha$ (F656N) image. The beam size of each map has been matched to $0''.43 \times 0''.41$, P.A. = 82° . Contours are half-integral powers of $\pm 2 \times 0.11$ and 0.17 for 6 and 2 cm, respectively. Uncertainty in the registration of the VLA and *HST* maps is $\sim 1''$.

source in the 2 cm map, assuming that the sources are Gaussian. (They are probably not Gaussian in structure, but this gives us approximate source sizes.) Uncertainties in the sizes, due to beam size, source structure, and signal-to-noise ratio, are $\lesssim 30\%$ of the beam. The derived source sizes in IC 342, Maffei II, and NGC 2903 are $\sim 0''.3$ but $\sim 0''.5$ in NGC 6946. Sources with larger deconvolved sizes in NGC 6946 are nebulae joined with the large emission complex at the center and suffer from confusion. Seeing may be a problem at 2 cm. The similarity of the source sizes suggest this may be the case; it is likely, therefore, that the sizes we obtain are upper limits to the true source sizes.

The deconvolved sizes correspond to diameters of ~ 6 – 14 pc. These $H\ II$ regions are significantly smaller than the 30 Dor $H\ II$ region (~ 200 pc in diameter for the region of $EM > 10^4$ pc cm^{-6} ; see Mills et al. [1978] and Kennicutt [1984]) in the Large Magellanic Cloud (LMC). They are larger but similar in nature to the Galactic compact $H\ II$ regions in W49 (Mezger et al. 1967; Conti & Blum 2002) and NGC 3603 (de Pree et al. 1999; Sung & Bessell 2004; Mücke et al. 2002). One possibility for the fact that these $H\ II$ regions are relatively compact and dense is that they are younger than 30 Dor or NGC 3603. Because these regions are nearly unresolved and we do not have good radio

spectral energy distributions, at this stage we cannot model their properties with precision.

The estimated sizes of these nebulae are similar to the parsec-sized diameters of the supernebulae found in NGC 5253 and II Zw 40 (Turner & Beck 2004; Beck et al. 2002; Meier et al. 2002). These $H\ II$ regions have ionized gas densities at least as high as $n_i \sim 10^3$ – 10^5 cm^{-3} ; they are dense, with high pressures. The compactness of these optically thick $H\ II$ regions implies some degree of youth, although $H\ II$ regions around massive young clusters may differ dynamically and evolve differently from Galactic compact $H\ II$ regions (Kroupa & Boily 2002; Turner et al. 2003; Turner & Beck 2004).

The radio fluxes of these compact $H\ II$ regions require that they harbor hundreds of massive stars. The luminosities of the clusters exciting the $H\ II$ regions can be inferred from their Lyman continuum rates using $L_{OB} = (2 \times 10^{-44}) N_{LyC}$ for a Salpeter initial mass function (IMF). The inferred luminosities are not very sensitive to IMF, since luminosity, like ionizing photons, is dominated by the most massive stars. The cluster luminosities inferred from the free-free emission are $\sim 10^8$ – $10^9 L_\odot$. Based on their luminosities, the largest of these radio clusters have roughly an order of magnitude more stars than the R136 cluster within

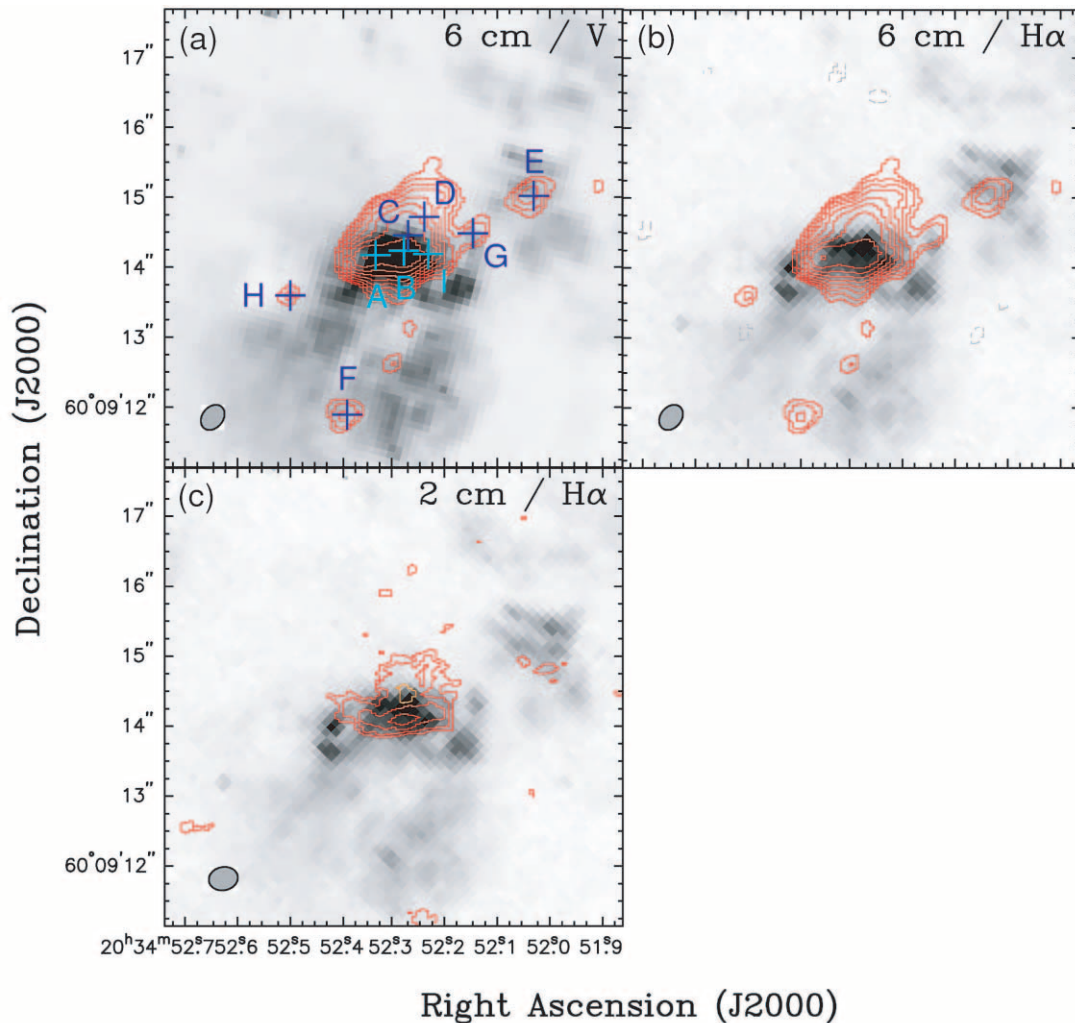


FIG. 5.—Close-ups of the center region of NGC 6946. (a) 6 cm contours overlaid on a WFPC2 V -band (F606W) image. (b) 6 cm contours overlaid on a WFPC2 $H\alpha$ (F656N) image. (c) 2 cm contours overlaid on a WFPC2 $H\alpha$ (F656N) image. The orange contour represents the region of decreasing flux density toward the center. The beam size of each map has been matched to $0''.42 \times 0''.38$, P.A. = -79° . Contours are at half-integral powers of $\pm 2 \times 0.10$ and 0.50 mJy beam $^{-1}$ for the 6 and 2 cm maps, respectively. Uncertainty in the registration of the VLA and *HST* maps is $\sim 1''$.

30 Dor (Massey & Hunter 1998; Zinnecker et al. 2002) or in the clusters within the large Galactic $H\ II$ region NGC 3603 (Eisenhauer et al. 1998; de Pree et al. 1999) or W49 (Conti & Blum 2002).

The total Lyman continuum rate, N_{Lyc} , is derived from the total flux from thermal compact sources, assuming the emission is optically thin and the $H\ II$ regions are ionization-bounded. These values are compared with N_{Lyc} rates derived from millimeter continuum, which are unlikely to suffer from opacity effects. In IC 342, the estimated N_{Lyc} is $\sim 6 \times 10^{51} \text{ s}^{-1}$ for six thermal compact sources. This can be compared with the values of $N_{\text{Lyc}} \sim 3 \times 10^{52} \text{ s}^{-1}$ obtained by Meier & Turner (2001; corrected for distance) for the central $16''$ region derived from 2.6 mm continuum and $N_{\text{Lyc}} \sim 1.2 \times 10^{52}$ for the two major 2.6 cm peaks corresponding to the central starburst regions. Over the central $7'' \times 2''$ region of NGC 6946, N_{Lyc} is $(3 \pm 0.2) \times 10^{52} \text{ s}^{-1}$, as derived from the 2.7 mm images of Meier & Turner (2004b; corrected to our distance). Similar agreement is also found in Maffei II between the N_{Lyc} value inferred by thermal fluxes in millimeters (D. S. Meier et al. 2006, in preparation) and centimeters (this work). These numbers imply that the fluxes of compact sources make up at least 50% of the total N_{Lyc} photons

seen toward the starburst peaks in lower resolution images. The fact that the millimeter emission gives higher values for N_{Lyc} suggests that some of the thermal sources are optically thick at centimeter wavelengths, or that some of the thermal flux is extended, or both.

4.2.2. Compact Nebulae and Molecular Clouds: Possible Star Formation Triggers

The existence of massive stars within these clusters indicates their youth. Because local star formation is expected to be suppressed by massive star feedback of mechanical energy through winds and supernovae, we expect the stars in these large clusters to be coeval to within a few megayears. Thus, they are presumably located inside and comoving with their parent molecular clouds and should be close to the sites at which they formed. Given that these $H\ II$ regions are compact and quite dense, it is likely that they may be significantly younger than the ~ 10 Myr we might infer from the presence of massive stars.

The young, massive clusters in IC 342 and Maffei II (shown in Figs. 2 and 3) are aligned with dust lanes and molecular gas. These nebulae are found in coherent structures extending over regions 110 pc (IC 342) to 240 pc (Maffei II) in size. The sound

TABLE 4
COMPACT CONTINUUM SOURCE-DERIVED PROPERTIES

Source (1)	α_{6-2}^a (2)	Type (3)	Free-Free τ (4)	$N_{\text{Lyc}}^{\text{thin } b}$ (10^{51} s^{-1}) (5)	N_{O7}^c (6)	L_{IR}^d ($10^7 L_{\odot}$) (7)	Comments (8)
IC 342							
A.....	$-0.5^{+0.2}_{-0.4}$	SNR	N/A
B.....	$-0.6^{+0.4}_{-0.5}$	SNR	N/A
C.....	$0.5^{+0.2}_{-0.2}$	H II	Thick	2.1	210	4.2	...
D.....	<-1.5	SNR/RSN	N/A
E.....	$0.0^{+0.5}_{-0.5}$	H II?	Thin?	0.7	70	1.4	...
F.....	<-0.6	SNR	N/A
G.....	$-0.3^{+0.6}_{-0.8}$	SNR	N/A
H.....	<-0.5	SNR	N/A
I.....	>1.1	H II	Thick	0.7	70	1.4	...
J.....	>1.1	H II	Thick	0.7	70	1.4	...
K.....	>1.1	H II	Thick	0.7	70	1.4	...
L.....	>1.1	H II	Thick	0.7	70	1.4	...
Total	5.6	560	11.1	...
Maffei II							
A.....	$-0.1^{+0.1}_{-0.1}$	H II	Thin	6.1	610	12.2	...
B.....	<-1.2	SNR/RSN	N/A
C.....	$0.3^{+0.2}_{-0.2}$	H II	Thick	4.9	490	9.7	...
D.....	$0.2^{+0.2}_{-0.3}$	H II	Thin?	4.1	410	8.2	...
E.....	$0.4^{+0.3}_{-0.3}$	H II	Thick?	2.9	290	5.8	...
F.....	$-0.4^{+0.2}_{-0.2}$	SNR	N/A
G.....	$0.2^{+0.2}_{-0.2}$	H II	Thin?	3.4	340	6.8	...
H.....	$0.3^{+0.3}_{-0.4}$	H II	Thick?	3.2	320	6.5	...
I.....	$-0.1^{+0.5}_{-0.7}$	H II?	Thin?	1.9	190	3.7	...
J.....	<-0.7	SNR	N/A
Total	26	2600	53	...
NGC 2903							
A.....	$0.0^{+0.3}_{-0.3}$	H II?	Thin?	2.9	290	5.8	...
B.....	$0.8^{+0.3}_{-0.3}$	H II	Thick	8.2	820	16	...
C.....	$-0.2^{+0.3}_{-0.4}$	H II	Thin?	2.3	230	4.6	...
D.....	<-0.5	SNR	N/A
E.....	$0.6^{+0.4}_{-0.4}$	H II	Thick	2.9	290	5.8	...
F.....	>1.2	H II	Thick	3.1	310	6.1	...
G.....	>1.0	H II	Thick	2.1	210	4.2	...
Total	21	2100	43	...
NGC 6946							
A ^e	$-0.3^{+0.2}_{-0.2}$	SNR?	N/A
B ^e	$0.1^{+0.1}_{-0.2}$	H II?	Thin?	4.5	450	9.0	...
C ^e	<-0.4	SNR?	N/A	Hole at 2 cm
D ^e	$0.0^{+0.2}_{-0.2}$	H II?	Thin?	3.0	300	6.0	...
E.....	$0.0^{+0.4}_{-0.4}$	H II?	Thin?	1.5	150	2.7	...
F.....	<0.3	?	Undetermined
G.....	<0.3	?	Undetermined
H.....	<0.3	?	Undetermined
I ^e	>1.1	H II	Thick	4.5	450	9.1	...
Total	14	1400	27	...

^a Spectral indices are computed from the total flux densities. The upper and lower limits are based on $\sqrt{2} \sigma$ release at both wavelengths.

^b Assume the electron temperature $T_e = 10,000$ K. The values will be $\sim 15\%$ lower than listed if $T_e = 6000$ K is assumed.

^c Assume the ionization rate of a reference O star, $N_{\text{O7}} \approx N_{\text{Lyc}} / 10^{49} \text{ s}^{-1}$.

^d Using $L_{\text{IR}}/N_{\text{Lyc}} = 2 \times 10^{-44} L_{\odot} \text{ s}$ for a L_{IR} estimate, based on ZAMS cluster (following Turner et al. 1998) and assuming $L_{\text{IR}} = L_{\text{OB}}$.

^e Confused sources. The α values are derived from peak fluxes. The $N_{\text{Lyc}}^{\text{thin}}$, N_{O7} , and L_{IR} values might be overestimated due to possible contamination in peak flux measurements by extended emission.

crossing times for these distances are 10–25 Myr if the sound speed is $\sim 10 \text{ km s}^{-1}$. This timescale is comparable to or longer than the lifetimes of massive stars. From the youth inferred from the high gas densities and from the spatial distribution of these H II regions along the CO arms, we conclude that the formation of young, massive stellar clusters in compact nebulae found in IC 342 and Maffei II is mainly triggered by large-scale resonant features (i.e., gas arms associated with spiral density wave/bar features; Lo et al. 1984; Ishizuki et al. 1990; Ishiguro et al. 1989; Hurt & Turner 1991; Schinnerer et al. 2003; Meier & Turner 2004a, 2005). This is consistent with their locations with respect to optical dust lanes (Figs. 2–5).

Comparing with the *HST* images (Figs. 2–5), we find that only a small fraction of the radio H II regions have possible optical counterparts. The extinction in embedded H II regions is often internal to the nebulae (Beck et al. 1986; Kawara et al. 1989; Ho et al. 1990), but it is also possible that the compact nebulae are hidden behind the foreground clouds or embedded in their host giant molecular clouds (GMCs). If we assume that all of the luminosity comes out in the IR, the implied L_{IR} of our compact sources amounts to only 3%–5% of the total IR luminosities of the galaxies (Table 1).

The young nebulae are all located within the central $\sim 100 \text{ pc}$ except in Maffei II, where the H II regions extend over $\sim 250 \text{ pc}$. To support the formation of numerous massive stars, there should be high molecular gas concentrations (Young & Scoville 1991). In all four galaxies, the central regions have molecular gas surface densities 3–9 times higher (Hurt & Turner 1991; Turner & Hurt 1992; Meier & Turner 2001, 2004b) than do typical spiral galaxies on size scales of $6''$ (Helfer et al. 2003). The high concentrations of molecular gas ($\Sigma_{\text{gas}} = 600\text{--}2000 M_{\odot} \text{ pc}^{-2}$ within the central $6''$; Hurt & Turner 1991; Helfer et al. 2003) lead to high internal visual extinctions A_V of up to tens to hundreds of magnitudes (Ho et al. 1990; Hurt & Turner 1991; Turner & Hurt 1992) toward these galactic centers.

The young star clusters associated with the radio nebulae are preferentially found projected onto the centers of GMCs (§ 4.3). This means that there is a wealth of gas around the star clusters to fuel more star formation, unlike the high star formation efficiency inferred from the lack of gas in the SSCs found in the dwarf galaxy NGC 5253 (Turner et al. 1997, 2002; Meier et al. 2002). Given the proximity of molecular clouds to these clusters and their location in the centers of large spiral galaxies, it is unlikely that any of the young clusters associated with the radio nebulae in these four spirals will become long-lived, gravitationally bound clusters, i.e., globular clusters.

4.3. Upper Part of the Luminosity Function of Young H II Regions

Nearly two dozen radio sources in the four galaxies were found to have flat or rising spectra (Table 4). These are presumably thermal nebulae excited by massive stars, for which the 2 cm fluxes give a lower limit to the required N_{Lyc} (§ 4.1). In Figure 6 we show the Lyman continuum luminosity function (LF) of these H II regions. The corresponding $H\alpha$ luminosities have been calculated from N_{Lyc} assuming no extinction, for comparison with other studies. The sample is small, and the statistical error bars are relatively large. However, there are some trends that appear to be real and should be studied with a larger sample.

We have fitted the LF with a power law and also with a two-component power law. The two-component fit is significantly better than the single-component fit. The LF has a steeper slope for nebulae with $H\alpha$ luminosity $> 2 \times 10^{39} \text{ erg s}^{-1}$ (corresponding

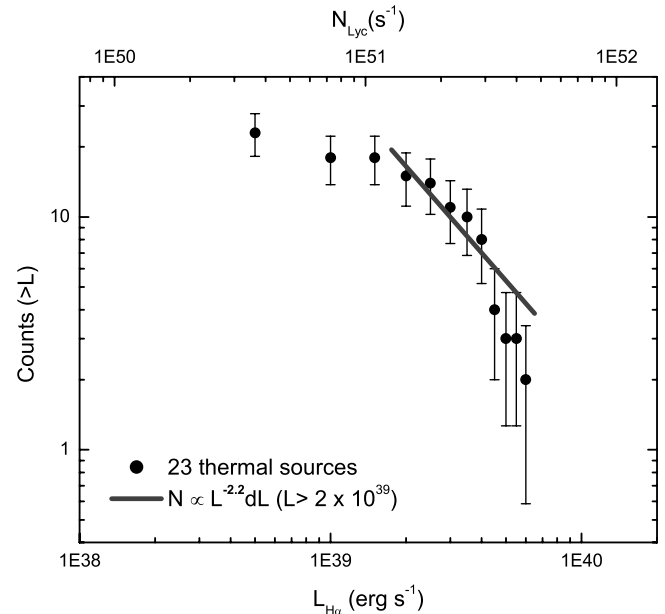


FIG. 6.—LF of the compact H II regions in the centers of IC 342, Maffei II, NGC 6946, and NGC 2903. Circles with statistical error bars show the cumulative number counts of H II regions found in the four spiral galaxies of our sample. The solid line represents the best-fit LF model for sources with $L_{H\alpha} > 2 \times 10^{39} \text{ erg s}^{-1}$. The sample is complete down to $N_{\text{Lyc}} \sim 6 \times 10^{50} \text{ s}^{-1}$ ($H\alpha \sim 8.3 \times 10^{38} \text{ erg s}^{-1}$). Each O7 star contributes roughly $N_{\text{Lyc}} \sim 10^{49} \text{ s}^{-1}$; the brightest sources (in Maffei II and NGC 2903) correspond to clusters of $\sim 500\text{--}1000$ O stars.

to $L_{\text{OB}} = 10^{7.5} L_{\odot}$, about 150 O7 stars). The line in Figure 6 represents power-law models [$N(L) \propto L^a dL$] of the LF with an index of -2.2 . The power-law index we obtain is close to the average value of -2.0 in 30 nearby spiral and irregular galaxies from an optical study of H II regions by Kennicutt et al. (1989). However, the slope of the LF for the more luminous H II regions of our sample is shallower than the slope in the two-component power-law LF, or “type II” LF, found in optical studies of other spiral galaxies, M51, NGC 3521, NGC 3627, NGC 4736 (Kennicutt et al. 1989), and NGC 7714 (Gonzalez-Delgado et al. 1995). The optical studies also show the turnover point at lower luminosity (at $L_{H\alpha} \sim 10^{38.7}\text{--}10^{39}$). A possible explanation for this difference might be that the luminous sources we found are very young and obscured and thus are not detected in the optical, although this may also be due to small-number statistics.

The flattening of the LF at the faint end may be caused by incompleteness due to both limited sensitivity and partially resolving out extended H II regions. We cannot detect unresolved (diameter $< 15 \text{ pc}$) nebulae with $N_{\text{Lyc}} < 4 \times 10^{50} \text{ s}^{-1}$ (3σ), corresponding to 40 O stars in IC 342 and 120 stars in NGC 6946. However, we also cannot detect more luminous but lower brightness regions if they are large and resolved (size $\gg 15 \text{ pc}$); in this limit we are sensitive to H II regions with $\text{EM} > 10^4 \text{ cm}^{-6} \text{ pc}$.

We did the same thermal source identification and $H\alpha$ luminosity calculation for radio sources in M 82, another nearby starburst galaxy, based on radio studies of Allen (1999). Allen’s source list is more complete, with $N_{\text{Lyc}} < 2 \times 10^{50} \text{ s}^{-1}$ (20 O7 stars) and radio nebulae with size $\lesssim 50 \text{ pc}$. The LF of the 21 sources in M82 with flat or rising spectra between 2 and 6 cm shows very similar features in slope and the break point in LF to what we find in the four spiral galaxies (Tsai et al. 2006). The agreement of LF shape of M82 and our sample suggests that the broken power law may be real. Larger samples would help to clarify this issue.

The steep power-law LF suggests a cutoff at the high-luminosity end in the young clusters associated with radio nebulae in spiral galaxies. The upper end of the LF is around $L_{\text{H}\alpha} \sim 10^{40}$ ergs s^{-1} . This corresponds to ~ 750 O7 stars. We observe two such clusters, in Maffei II and NGC 2903, and their nebulae are $\lesssim 5$ pc in extent. The total mass of such a cluster would be $\sim 2.2 \times 10^5 M_{\odot}$ (assuming a Salpeter IMF), consistent with the masses of Galactic globular clusters.

5. INDIVIDUAL GALAXIES

5.1. IC 342

IC 342 is a face-on giant Scd spiral galaxy (Ables 1971; Crosthwaite et al. 2000, 2001) close to the Galactic plane. Its distance is uncertain: Saha et al. (2002) used the P - L relation for Cepheids and suggested 3.3 Mpc, close to the 3.9 Mpc given by Tully & Fisher (1988), but earlier measurements found ~ 2 Mpc in optical spectroscopic and photometric studies (McCall 1989; Karachentsev & Tikhonov 1993). Here we adopt 3.3 Mpc ($1'' = 16$ pc).

The core of IC 342 contains a central molecular ring $5''$ – $6''$ in radius and a nuclear CO disk $\sim 3''5$ (~ 55 pc) in diameter (Schinnerer et al. 2003). The $5''$ – $6''$ nuclear disk contains $\sim 2 \times 10^5 M_{\odot}$ of molecular gas, and the central 100 pc contains $\sim 5 \times 10^6 M_{\odot}$ of molecular gas (Meier & Turner 2001). The nuclear star cluster (NSC) of IC 342 has been studied in optical and IR wavelengths using *HST* and the Infrared Telescope Facility. The NSC of IC 342 has a mass of $M \approx 6 \times 10^6 M_{\odot}$ and an age of $10^{6.8}$ – $10^{7.8}$ yr. The upper limit on a central black hole is $5 \times 10^5 M_{\odot}$ (Böker et al. 1999). Outside the central star cluster, there is current star formation indicated by bright IR and radio emission clumps, each containing 10^2 – 10^3 OB stars, and the total number of equivalent O stars is about 5000 (Becklin et al. 1980; Turner & Ho 1983). Our measurements resolve out most of the extended component of emission, so our calculated total O star population, which detects compact sources only, is over an order of magnitude less.

The radio continuum images (Fig. 2) reveal 12 compact radio continuum sources on the two spiral arms and the central molecular ring of IC 342. Ten percent of the total radio emission at 6 cm and 20% at 2 cm for the central kiloparsec arises in compact sources. Inferring the IR luminosities from their radio fluxes and $N_{\text{Lyc}} (L_{\text{OB}})$, we find that the compact H II regions in the nucleus contribute only $\sim 5\%$ of the total IR luminosity of IC 342. Two-centimeter sources, A, C, E, G, and I–K, are distributed along the inner edge of the dust lane and the western molecular spiral arm near the nucleus (Schinnerer et al. 2003). The western arm of the central molecular ring clearly has more energetic star formation than the eastern arm, as is evident from lower resolution observations. The star formation in IC 342 appears to be spatially distributed in the nuclear region, although somewhat concentrated to the west near the northern end of the western molecular arm (Meier & Turner 2005).

We identify a number of likely SNRs. Source G in the eastern central molecular arm has $\alpha \sim -0.3$. Four sources, B, D, F, and H, are detected only at 6 cm. Sources A and B have $\alpha \sim -0.5$ and -0.6 , respectively, close to the conventional α of Galactic SNRs. The steep spectrum of source D makes it a candidate for a RSN, which typically declines rapidly over the span of a few years. However, no obvious change in the 6 cm flux of source D is found in the data of IC 342 we have collected over multiple epochs separated over 15 yr. Its diameter ($\sim 0''.6$ – $0''.4$, or 10–6 pc) and luminosity $L_{6 \text{ cm}} = 2.9 \times 10^{19}$ ergs $\text{s}^{-1} \text{ Hz}^{-1}$ can be explained better by a SNR. The unusual negative spectral index of

source D might be due to the flux contamination by nearby nonthermal source F. Sources F and H show no strong emission at 2 cm and have upper limits to their spectral indices of $\alpha < -0.5$. None of these sources, A, B, D, or F–H, are associated with obvious visible star clusters. As SNR candidates, they are the likely end stages of massive stars near the young star cluster systems.

We identify five compact sources that appear to be compact H II regions. Sources C, I, J, and K in the northwest and source L in the east have spectra consistent with optically thick free-free emission. If the emission were optically thin, the excitation of these compact nebulae would require clusters of at least 70–210 O7 stars each. These are lower limits to the true cluster population, because the emission is optically thick and because of the possibility of dust absorption of the UV photons. The inferred cluster masses are then $(2.1$ – $6.3) \times 10^4 M_{\odot}$. These are large clusters comparable to or a few times larger than 30 Dor in the LMC, but much more compact. These nebulae are less than 8 pc in size as compared to 200 pc for 30 Dor, and hence probably younger. These star clusters are not detected in the *HST* image, implying that $A_V \gtrsim 5$ mag, or $N_{\text{H}} \gtrsim 1.0 \times 10^{22} \text{ cm}^{-2}$, if zero-age main sequence (ZAMS) star clusters with Salpeter IMF are assumed. The $4''$ resolution $10 \mu\text{m}$ image of IC 342 (Becklin et al. 1980) shows two peaks at $\sim \alpha = 03^{\text{h}}46^{\text{m}}48^{\text{s}}.3$, $\delta = +68^{\circ}05'47''$ and $\sim \alpha = 03^{\text{h}}46^{\text{m}}47^{\text{s}}.6$, $\delta = +68^{\circ}05'46''$, close to the radio H II regions we identify here. The visual extinction estimated from the silicate absorption feature is ~ 15 mag toward these two $10 \mu\text{m}$ peaks (Becklin et al. 1980), consistent with our argument of high extinction toward these H II regions.

To the west, source E has a flatter radio spectrum and appears to be an optically thin source. This H II region requires about 70 O stars, comparable to 30 Dor. A ZAMS star cluster with 70 O stars in IC 342 should have apparent brightness $m_V = 13.8$ when Galactic extinction of $A_V = 1.85$ ($N_{\text{H}} \sim 3.5 \times 10^{21} \text{ cm}^{-2}$) toward IC 342 is applied; these clusters do not appear in the *HST* optical image (Fig. 3; also see Böker et al. 1999).

We do not detect significant radio continuum emission at small size scales from the NSC to a 3σ limit of $6.5 \times 10^{50} \text{ s}^{-1}$, or 70 equivalent O7 stars. This is consistent with a somewhat older stellar population there (60 Myr; Böker et al. 1999). No significant active galactic nucleus has been detected with these high-resolution measurements, but our own Galactic center at a similar resolution (Brown & Johnston 1983) would be below our detection limit at this distance (~ 0.1 mJy at 2 cm).

5.2. Maffei II

Maffei II, discovered in the IR by Maffei (1968), is a spiral galaxy with a strong and long bar evident in near-IR images (Hurt et al. 1993a). It is located behind the Galactic plane ($l = 136^{\circ}.50$, $b = -0^{\circ}.33$) at $A_V \sim 5$ – 10 mag of Galactic extinction. The nucleus of the galaxy comprises actively forming stars (Rickard & Harvey 1983; Ho et al. 1990; Telesco et al. 1993; Seaquist et al. 1976; Turner & Ho 1994). The distance of Maffei II was recently set at 2.8 Mpc by Karachentsev et al. (2003) using the Tully-Fisher relation; however, the H I line width suffers from Galactic absorption, particularly in lower resolution spectra (Hurt et al. 1996), so the actual H I line width is larger than what they adopt. In this paper we use the distance of 5 Mpc estimated from the diameters of the largest H II regions in Maffei II (Spinrad et al. 1973) and by the Tully-Fisher analysis of Hurt et al. (1993b). The uncertainty in the distance to Maffei II introduces a factor of 3 uncertainty in estimates of massive star numbers and total masses and a factor of 2 uncertainty in source sizes.

In Figure 3 we show the radio continuum maps of Maffei II. Ten sources are identified in both 2 and 6 cm maps, and sources B and J are identified only at 6 cm (see Table 3 and Fig. 3). The compact sources lie on a twisted, inverse S-shaped line north-south, following the trend of larger scale gas distribution and coinciding with the dust lane shown in the *HST* *V*-band image. The radio continuum emission is located along the elongated bar of 45'' length seen in the ^{12}CO (Ishiguro et al. 1989) and ^{13}CO (Hurt & Turner 1991) images. The northern sources B, C, and F are associated with GMC D1 of D. S. Meier et al. (2006, in preparation). Sources A, D, H, I, and J are close to the center of GMC E. The southern sources, E and G, are between GMCs E and F. Strong detections in both 6 and 2 cm provide good spectral indices and sizes for the radio sources in Maffei II, except for sources B and J, which have no significant detection at 2 cm.

The total flux densities from compact sources constitute $\sim 15\%$ of the total emission of the central kiloparsec of Maffei II at 6 cm and $\sim 30\%$ at 2 cm (for structures $< 45''$; see § 2). Turner & Ho (1994), using the VLA in the B configuration at 6 cm and C configuration at 2 cm, found a total number of O stars in good agreement with our results. The star formation in the center of Maffei II is concentrated in large, compact clusters aligned in a linear structure along the northern CO arm. The predicted IR luminosity $L_{\text{IR}} = L_{\text{OB}} \sim 5.3 \times 10^8 L_{\odot}$ from these point sources is $\sim 5\%$ of the total L_{IR} of Maffei II. Except for three SNR/RSN candidates, the compact radio continuum sources we detect are thermal free-free emission from H II regions. Most of the thermal sources in Maffei II have relatively flat spectra, compared with rising spectrum sources in NGC 2903 and NGC 6946.

Spectral indices $\alpha \sim -0.1$ for sources A, D, and I suggest that these are star clusters with optically thin thermal free-free radiation. All three are in the center of the radio emission near GMC D1. These H II regions of diameter ≤ 10 pc each require ~ 200 – 600 exciting O stars. The inferred masses of the clusters associated with sources C and G are $\sim (6$ – $18) \times 10^4 M_{\odot}$, slightly larger than the young massive star clusters in our Galactic center.

Sources C, E, G, and H have rising spectra indicating that they are compact H II regions. These H II regions are brighter and more luminous than the ones in IC 342. The lower limit of $N_{\text{Lyc}} = (2.9$ – $4.9) \times 10^{51} \text{ s}^{-1}$ requires clusters of more than 300–500 O7 stars. The inferred cluster masses are $M_C \sim (1$ – $1.5) \times 10^5 M_{\odot}$. The mass of source C, $M_C \sim 1.5 \times 10^5 M_{\odot}$, is only a small fraction of the $26 \times 10^6 M_{\odot}$ upper limit mass of GMC C (D. S. Meier et al. 2006, in preparation). The star formation efficiency therefore appears to be of order 1%, which is similar to the Galactic value on these scales. From the $\text{C}^{18}\text{O}(2$ – $1)$ map of D. S. Meier et al. (2006, preparation), sources E and G seem to be at the gas bridge in the middle of GMC D1 and GMC E3. The predicted visual brightness of these rising spectrum sources with the assumption of a Salpeter IMF is $m_V \sim 25$ mag with Galactic extinction, so these sources are too faint and highly obscured to be detected via *HST* observations.

Source F is probably a SNR, with $\alpha = -0.4$. The luminosity of source F at 6 cm is $L_{6 \text{ cm}} \sim 4.6 \times 10^{25} \text{ ergs s}^{-1} \text{ Hz}^{-1}$, and the deconvolved size is 11×8 pc, characteristic of a young Type II SNR. Sources B and J show no significant counterpart at 2 cm, and their negative spectral indexes suggest that they are a RSN and SNR, respectively. All three nonthermal sources, F, B, and J, are within $\geq 1''$ (25 pc in projection) of the nearby optically thick thermal sources, C and H. The locations of these SNR/RSN candidates suggest that they might be associated with the compact H II regions.

5.3. NGC 2903

NGC 2903 is a large and bright “hot-spot” spiral galaxy with an unusually complex structure of both early- and late-type stars and H II regions at its center (Oka et al. 1974; Sérsic & Pastoriza 1967; Morgan 1958; Sérsic 1973). It is at a distance of 8.9 Mpc (Drozdovsky & Karachentsev 2000). Wynn-Williams & Becklin (1985) studied the hot-spot galaxy in the radio and IR and found that its radio emission is predominantly nonthermal. However, in some regions the free-free emission contributes substantially at 2 cm. NGC 2903 has a well-studied star-forming ring. IR maps find H II regions in the ring with luminosities approaching that of 30 Dor (Alonso-Herrero et al. 2001). IR spectroscopy gives an age range of $(4$ – $7) \times 10^6$ yr for the embedded star clusters, while the H II regions are thought to be only $(1$ – $4) \times 10^6$ yr of age (Alonso-Herrero et al. 2001). Molecular gas in NGC 2903 is concentrated in the central few tens of arcseconds (Sheth et al. 2002; Helfer et al. 2003).

In Figure 4 we show NGC 2903 in radio continuum maps and *HST* WFPC2 images (*V* band and $\text{H}\alpha$). About 20% of the total flux density at 2 cm emission in the central kiloparsec comes from the compact sources B, C, E, F, and G. At 6 cm $\sim 5\%$ is due to sources A–E. This agrees with Wynn-Williams & Becklin (1985) on the contribution of compact sources at radio wavelengths. The northern peak near $\alpha = 09^{\text{h}}32^{\text{m}}09^{\text{s}}.99$, $\delta = 21^{\circ}30'12''.7$ seen in low-resolution 2 cm maps (Wynn-Williams & Becklin 1985) does not have a corresponding compact source in our images and therefore must be extended over $> 2''$ scales.

The *K*- and *H*-band NICMOS and $\text{Pa}\alpha$ images of the nucleus of NGC 2903 (Alonso-Herrero et al. 2001) show an absence of ionized gas, consistent with what is seen in our 2 and 6 cm maps. The nucleus must consist of a relatively old stellar population dominated by giant and supergiant stars. The northern peak of the lower resolution 2 cm maps of Wynn-Williams & Becklin (1985) corresponds to compact source B. It has a rising spectrum of $\alpha \sim 0.8$ through centimeter wavelengths. Excitation of source B requires at least 800 O7 stars if the free-free emission is thin and more if thick. This result is ~ 2.6 times higher than N_{Lyc} derived by Alonso-Herrero et al. (2001). It suggests visual extinctions of 2.7 mag, higher than what Alonso-Herrero et al. (2001) obtained, and thus $A_V = 6.5$, assumed if $A_V/A_{1.87 \mu\text{m}}$ applied (Cardelli et al. 1989). This difference could be explained if there is significant extinction at $\text{Pa}\alpha$. The brightness temperature of source B indicates a size of $0''.025$, or 1.1 pc for a nebula with $T_e = 10,000$ K. Source B is a good candidate for a SSC nebula.

Sources A, D, E, and G are within the extended emission east of the northern peak (Wynn-Williams & Becklin 1985) near source B. All of them have counterparts in $\text{Pa}\alpha$ (Alonso-Herrero et al. 2001), except source E. Source E is close to source “b” of Oka et al. (1974), which they claim to be a free-free emitter. Source E also appears coincident with cluster 2 in the *HST* near-IR images (Alonso-Herrero et al. 2001) and the AO *K'*-band image (Pérez-Ramírez et al. 2000). Sources A, B, D, and G correspond to sources H1, H4, H2, and H3 of Pérez-Ramírez et al. (2000), respectively. In our maps, source G has been identified only at 2 cm and shows a very steep rising spectrum. Its spectral index, $\alpha > 1.0$, implies that this is a possible compact H II region with a high electron density and should therefore be very young. Source D, detected at 6 cm but not at 2 cm, is probably a SNR. Source A has a flat slope of $\alpha \sim 0.0 \pm 0.3$. It could be a small H II region, with ~ 210 equivalent O stars, or, within the uncertainties, it could also be a single young Crab-like SNR with the luminosity of Cas A.

The southern sources C and F have thermal spectra. Source C coincides with the southern peak in the low-resolution 2 cm map of Wynn-Williams & Becklin (1985). The flux density at 2 cm is about a quarter of the peak in the C configuration maps, so this source is extended. Source C contains about 230 O stars in $0''.4 \times 0''.3$ based on its 2 cm flux and 100 equivalent O stars based on the Pa α measurement of Alonso-Herrero et al. (2001); the discrepancy is probably due to extinction at Pa α . Source F is an optically thick H II region with spectral index $\alpha > 1.2$. The cluster inferred to be exciting source F has $L_{\text{OB}} \sim 1.6 \times 10^8 L_{\odot}$ and mass $M_C < 2.3 \times 10^5 M_{\odot}$, which is about the mass of a globular cluster.

5.4. NGC 6946

NGC 6946 is a barred spiral galaxy close to the Galactic plane ($l = 95^{\circ}72$, $b = 11^{\circ}67$). It is a bright mid-IR (Rieke & Lebofsky 1978), CO (Ball et al. 1985; Sofue et al. 1988; Weliachew et al. 1988; Casoli et al. 1992; Regan & Vogel 1995; Sakamoto et al. 1999), and radio (Turner & Ho 1983) source. NGC 6946 contains a moderate starburst of $L_{\text{IR}} \sim 2.2 \times 10^9 L_{\odot}$, age range 7–20 Myr (Engelbracht et al. 1996), and $1 \times 10^8 M_{\odot}$ of molecular gas, concentrated in the central 175 pc (Meier & Turner 2004b). The distance to NGC 6946 is estimated at 5.5 Mpc (Tully & Fisher 1988), to 5.9 ± 0.4 Mpc (Karachentsev et al. [2000] based on blue supergiants); we adopt 5.9 Mpc.

In Figure 5 we show the radio continuum maps and the V -band and H α *HST* WFPC2 images of NGC 6946. They were registered by aligning the 6 cm peak and V -band and H α peak. We identify five sources with intensity peaks in the emission complex, A–D and I, in the central 60 pc of NGC 6946. The most luminous 2 cm source, source B, is considered to have the strongest H α emission. These five sources appear related to GMC E1 in Meier & Turner (2004b), a cloud that has a molecular gas mass of $14 \times 10^6 M_{\odot}$. Sources E, F, and H are farther away from the center and are detected only at 6 cm. They have no optical counterparts, although E might be associated with the diffuse optical emission northwest of the optical peak. These nine compact sources contribute 30% of the total 6 cm emission and 30% of the 2 cm emission from the central kiloparsec of this galaxy. The high fraction of 6 cm emission from compact sources as compared with the other three spiral galaxies suggests that there are compact and young SNRs in the center of NGC 6946, which may have a more evolved star cluster than the other spiral galaxies.

Sources A–D and I are within $2''$, or 60 pc in projection, of the peak in the *HST* V -band image. The IR peak shown in an archived NICMOS F160W image lies on source I to within the pointing uncertainties of *HST*. Even with subarcsecond resolution, we cannot resolve the extended emission between these sources. We derive their spectral indices based on their peak fluxes. It is possible that they are physically connected to each other and that the two nonthermal sources, A and C, are the consequence of extensive star formation near sources B, D, and I. The optical peak of NGC 6946 is associated with the 12–15 Myr old cluster 1094 (Larsen et al. 2002) of $M_V = -10.18$ mag, which is comparable in luminosity to the bright open star clusters but inconspicuous in comparison with a young SSC. By comparison, source B, D, and I together should have $M_V \sim -12.5$ mag. Using the column density of molecular hydrogen derived from CO (Meier & Turner 2004b), we estimate that $A_V \sim 20$ –30 mag

toward sources D and I. Sources B, D, and I are probably embedded in GMC E1.

Sources A and C have negative spectra and are likely SNRs (Weiler et al. 1986). The 2 cm map shows a decrease in flux density at the position of source C. This suggests the contamination from extended emission might be responsible for the SNR-like spectral index of these two sources. Thus, we cannot distinguish them from RSNe, SNRs, or H II regions. They could be explained by one or a few short-lived young Type I RSNe (Weiler et al. 1998).

Source E shows extended emission at 2 cm and is marginally detected. In Table 4 we put its peak and integrated fluxes at 2 cm in the area of the 6 cm beam. The flat spectrum suggests that source E is a large (30 Dor–like) H II region. We do not have significant detections toward sources F–H at 2 cm and cannot identify their nature.

6. CONCLUSIONS

We have imaged compact radio emission in the centers of four nearby spiral galaxies, IC 342, Maffei II, NGC 2903, and NGC 6946, at subarcsecond resolution at 6 and 2 cm with the VLA. Compact radio sources contribute $\sim 20\%$ – 30% of the total 2 cm emission from the central kiloparsec of these galaxies, but only 5%–10% at 6 cm; in NGC 6946, they contribute $\sim 30\%$ at both wavelengths. The 2 cm emission within the central 100–200 pc of these spiral galaxies is dominated by H II regions, while diffuse synchrotron emission dominates at 6 cm. Over half of the 38 identified compact sources appear to be H II regions based on their radio spectra; of these, one-third to half appear to have optically thick free-free emission. The high resolution of these maps selects for these compact, high-brightness H II regions. The brightness temperatures of these optically thick, compact H II regions are consistent with this identification and indicate actual source diameters of about 1–3 pc ($\sim 0''.02$ – $0''.05$). The compact H II regions contain ionized gas with densities as high as $n_i \sim 10^4 \text{ cm}^{-3}$, which suggests that these H II regions are relatively young. Few of the compact radio sources have candidate counterparts in the visual wave bands. Comparison with optical *HST* images shows that the young H II regions tend to be found in dust lanes and probably are subject to high extinction and dynamical influences from molecular clouds. The predicted IR emission from these H II regions contributes 3%–5% of the total IR luminosity of the galaxies. The largest H II regions require the equivalent of ~ 500 – 1000 O7 stars to excite them; since they are dense, compact H II regions, by analogy with Galactic compact H II regions they are likely to be the very youngest of the massive young clusters, a megayear or less in age.

This research has been supported by NSF grants AST 03-07950 and AST 00-71276. Some of the data presented in this paper were obtained from the Multimission Archive at the Space Telescope Science Institute (STScI). STScI is operated by the Association of Universities for Research in Astronomy, Inc., under NASA contract NAS5-26555. This research has also made use of the NASA/IPAC Extragalactic Database and the NASA/IPAC Infrared Science Archive, which are operated by the Jet Propulsion Laboratory, California Institute of Technology, under contract with the National Aeronautics and Space Administration.

REFERENCES

- Ables, A. D. 1971, *Publ. USNO*, 20, 79
- Allen, M. L. 1999, Ph.D. thesis, Univ. Toronto
- Alonso-Herrero, A., Ryder, S. D., & Knapen, J. H. 2001, *MNRAS*, 322, 757
- Arp, H., & Sandage, A. 1985, *AJ*, 90, 1163
- Ball, R., Sargent, A. I., Scoville, N. Z., Lo, K. Y., & Scott, S. L. 1985, *ApJ*, 298, L21
- Beck, S. C., Turner, J. L., & Ho, P. T. P. 1986, *ApJ*, 309, 70
- Beck, S. C., Turner, J. L., & Kovo, O. 2000, *AJ*, 120, 244
- Beck, S. C., Turner, J. L., Langland-Shula, L. E., Meier, D. S., Crosthwaite, L. P., & Gorjian, V. 2002, *AJ*, 124, 2516
- Becklin, E. E., Gatley, I., Matthews, K., Neugebauer, G., Sellgren, K., Werner, M. W., & Wynn-Williams, C. G. 1980, *ApJ*, 236, 441
- Böker, T., Laine, S., van der Marel, R. P., Sarzi, M., Rix, H., Ho, L. C., & Shields, J. C. 2002, *AJ*, 123, 1389
- Böker, T., van der Marel, R. P., & Vacca, W. D. 1999, *AJ*, 118, 831
- Brown, R. L., & Johnston, K. J. 1983, *ApJ*, 268, L85
- Cardelli, J. A., Clayton, G. C., & Mathis, J. S. 1989, *ApJ*, 345, 245
- Casoli, F., Dupraz, C., & Combes, F. 1992, *A&A*, 264, 55
- Chini, R., Kreysa, E., Kruegel, E., & Mezger, P. G. 1986, *A&A*, 166, L8
- Condon, J. J. 1992, *ARA&A*, 30, 575
- Conti, P. S., & Blum, R. D. 2002, *ApJ*, 564, 827
- Crosthwaite, L. P., Turner, J. L., & Ho, P. T. P. 2000, *AJ*, 119, 1720
- Crosthwaite, L. P., Turner, J. L., Hurt, R. L., Levine, D. A., Martin, R. N., & Ho, P. T. P. 2001, *AJ*, 122, 797
- de Pree, C. G., Nysewander, M. C., & Goss, W. M. 1999, *AJ*, 117, 2902
- Drozdovsky, I. O., & Karachentsev, I. D. 2000, *A&AS*, 142, 425
- Eisenhauer, F., Quirrenbach, A., Zinnecker, H., & Genzel, R. 1998, *ApJ*, 498, 278
- Engelbracht, C. W., Rieke, M. J., Rieke, G. H., & Latter, W. B. 1996, *ApJ*, 467, 227
- Gonzalez-Delgado, R. M., Perez, E., Diaz, A. I., Garcia-Vargas, M. L., Terlevich, E., & Vilchez, J. M. 1995, *ApJ*, 439, 604
- Green, D. A. 1984, *MNRAS*, 209, 449
- Habing, H. J., & Israel, F. P. 1979, *ARA&A*, 17, 345
- Helfer, T. T., Thornley, M. D., Regan, M. W., Wong, T., Sheth, K., Vogel, S. N., Blitz, L., & Bock, D. C.-J. 2003, *ApJS*, 145, 259
- Ho, P. T. P., Beck, S. C., & Turner, J. L. 1990, *ApJ*, 349, 57
- Ho, P. T. P., Turner, J. L., Fazio, G. G., & Willner, S. P. 1989, *ApJ*, 344, 135
- Hurt, R. L., Merrill, K. M., Gatley, I., & Turner, J. L. 1993a, *AJ*, 105, 121
- Hurt, R. L., & Turner, J. L. 1991, *ApJ*, 377, 434
- Hurt, R. L., Turner, J. L., & Ho, P. T. P. 1996, *ApJ*, 466, 135
- Hurt, R. L., Turner, J. L., Ho, P. T. P., & Martin, R. N. 1993b, *ApJ*, 404, 602
- Ishiguro, M., et al. 1989, *ApJ*, 344, 763
- Ishizuki, S., Kawabe, R., Ishiguro, M., Okumura, S. K., & Morita, K.-I. 1990, *Nature*, 344, 224
- Karachentsev, I. D., Sharina, M. E., Dolphin, A. E., & Grebel, E. K. 2003, *A&A*, 408, 111
- Karachentsev, I. D., Sharina, M. E., & Huchtmeier, W. K. 2000, *A&A*, 362, 544
- Karachentsev, I. D., & Tikhonov, N. A. 1993, *A&AS*, 100, 227
- Kawara, K., Nishida, M., & Phillips, M. M. 1989, *ApJ*, 337, 230
- Kennicutt, R. C., Jr. 1984, *ApJ*, 287, 116
- Kennicutt, R. C., Jr., Edgar, B. K., & Hodge, P. W. 1989, *ApJ*, 337, 761
- Kobulnicky, H. A., & Johnson, K. E. 1999, *ApJ*, 527, 154
- Kroupa, P., & Boily, C. M. 2002, *MNRAS*, 336, 1188
- Larsen, S. S., Efremov, Y. N., Elmegreen, B. G., Alfaro, E. J., Battinelli, P., Hodge, P. W., & Richtler, T. 2002, *ApJ*, 567, 896
- Lo, K. Y., et al. 1984, *ApJ*, 282, L59
- Maffei, P. 1968, *PASP*, 80, 618
- Massey, P., & Hunter, D. A. 1998, *ApJ*, 493, 180
- McCall, M. L. 1989, *AJ*, 97, 1341
- McDonald, A. R., Muxlow, T. W. B., Wills, K. A., Pedlar, A., & Beswick, R. J. 2002, *MNRAS*, 334, 912
- Meier, D. S., & Turner, J. L. 2001, *ApJ*, 551, 687
- . 2004a, *BAAS*, 36, 1508
- . 2004b, *AJ*, 127, 2069
- . 2005, *ApJ*, 618, 259
- Meier, D. S., Turner, J. L., & Beck, S. C. 2002, *AJ*, 124, 877
- Mezger, P. G., & Henderson, A. P. 1967, *ApJ*, 147, 471
- Mezger, P. G., Schraml, J., & Terzian, Y. 1967, *ApJ*, 150, 807
- Mills, B. Y., Turtle, A. J., Little, A. G., & Durdin, J. M. 1984, *Australian J. Phys.*, 37, 321
- Mills, B. Y., Turtle, A. J., & Watkinson, A. 1978, *MNRAS*, 185, 263
- Morgan, W. W. 1958, *PASP*, 70, 364
- Moshir, M., et al. 1990, *BAAS*, 22, 1325
- Mücke, A., Koribalski, B. S., Moffat, A. F. J., Corcoran, M. F., & Stevens, I. R. 2002, *ApJ*, 571, 366
- Oka, S., Wakamatsu, K., Sakka, K., Nishida, M., & Jugaku, J. 1974, *PASJ*, 26, 289
- Pagel, B. E. J., Edmunds, M. G., Blackwell, D. E., Chun, M. S., & Smith, G. 1979, *MNRAS*, 189, 95
- Pérez-Ramírez, D., Knapen, J. H., Peletier, R. F., Laine, S., Doyon, R., & Nadeau, D. 2000, *MNRAS*, 317, 234
- Regan, M. W., & Vogel, S. N. 1995, *ApJ*, 452, L21
- Rickard, L. J., & Harvey, P. M. 1983, *ApJ*, 268, L7
- Rickard, L. J., Turner, B. E., & Palmer, P. 1977, *ApJ*, 218, L51
- Rieke, G. H., & Lebofsky, M. J. 1978, *ApJ*, 220, L37
- Sage, L. J., Shore, S. N., & Solomon, P. M. 1990, *ApJ*, 351, 422
- Saha, A., Claver, J., & Hoessel, J. G. 2002, *AJ*, 124, 839
- Sakamoto, K., Okumura, S. K., Ishizuki, S., & Scoville, N. Z. 1999, *ApJS*, 124, 403
- Sanders, D. B., & Mirabel, I. F. 1996, *ARA&A*, 34, 749
- Schinnerer, E., Böker, T., & Meier, D. S. 2003, *ApJ*, 591, L115
- Seaquist, E. R., Pfund, J., & Bignell, R. C. 1976, *A&A*, 48, 413
- Sedwick, K. E., & Aller, L. H. 1981, *Proc. Natl. Acad. Sci.*, 78, 1994
- Sérsic, J. L. 1973, *PASP*, 85, 103
- Sérsic, J. L., & Pastoriza, M. 1967, *PASP*, 79, 152
- Sheth, K., Vogel, S. N., Regan, M. W., Teuben, P. J., Harris, A. I., & Thornley, M. D. 2002, *AJ*, 124, 2581
- Sofue, Y., Doi, M., Ishizuki, S., Nakai, N., & Handa, T. 1988, *PASJ*, 40, 511
- Spinrad, H., Bahcall, J., Becklin, E. E., Gunn, J. E., Kristian, J., Neugebauer, G., Sargent, W. L. W., & Smith, H. 1973, *ApJ*, 180, 351
- Sung, H., & Bessell, M. S. 2004, *AJ*, 127, 1014
- Tarchi, A., Neininger, N., Greve, A., Klein, U., Garrington, S. T., Muxlow, T. W. B., Pedlar, A., & Glendenning, B. E. 2000, *A&A*, 358, 95
- Telesco, C. M., Dressel, L. L., & Wolstencroft, R. D. 1993, *ApJ*, 414, 120
- Telesco, C. M., & Harper, D. A. 1980, *ApJ*, 235, 392
- Tsai, C.-W., Beck, S. C., Crosthwaite, L. P., Ho, P. T. P., & Meier, D. S. 2006, preprint (astro-ph/0609210)
- Tully, R. B., & Fisher, J. R. 1988, *Catalog of Nearby Galaxies* (Cambridge: Cambridge Univ. Press)
- Turner, J. L., & Beck, S. C. 2004, *ApJ*, 602, L85
- Turner, J. L., Beck, S. C., Crosthwaite, L. P., Larkin, J. E., McLean, I. S., & Meier, D. S. 2003, *Nature*, 423, 621
- Turner, J. L., Beck, S. C., & Ho, P. T. P. 1999, in *IAU Symp. 193, Wolf-Rayet Phenomena in Massive Stars and Starburst Galaxies*, ed. K. A. van der Hucht, G. Koenigsberger, & P. R. J. Eenens (San Francisco: ASP), 758
- . 2000, *ApJ*, 532, L109
- Turner, J. L., Beck, S. C., & Hurt, R. L. 1997, *ApJ*, 474, L11
- Turner, J. L., Crosthwaite, L. P., Meier, D. S., Kovacs, A., Benford, D. J., & Beck, S. C. 2002, *BAAS*, 34, 1294
- Turner, J. L., & Ho, P. T. P. 1983, *ApJ*, 268, L79
- . 1994, *ApJ*, 421, 122
- Turner, J. L., Ho, P. T. P., & Beck, S. C. 1998, *AJ*, 116, 1212
- Turner, J. L., & Hurt, R. L. 1992, *ApJ*, 384, 72
- van der Hulst, J. M., Crane, P. C., & Keel, W. C. 1981, *AJ*, 86, 1175
- . 1983, *AJ*, 88, 138
- Verter, F. 1985, *ApJS*, 57, 261
- Weiler, K. W., Sramek, R. A., Panagia, N., van der Hulst, J. M., & Salvati, M. 1986, *ApJ*, 301, 790
- Weiler, K. W., van Dyk, S. D., Montes, M. J., Panagia, N., & Sramek, R. A. 1998, *ApJ*, 500, 51
- Weliachew, L., Casoli, F., & Combes, F. 1988, *A&A*, 199, 29
- Whitmore, B. C. 2003, in *A Decade of Hubble Space Telescope Science*, ed. M. Livio, K. Noll, & M. Stiavelli (Cambridge: Cambridge Univ. Press), 153
- Wood, D. O. S., & Churchwell, E. 1989, *ApJ*, 340, 265
- Wynn-Williams, C. G., & Becklin, E. E. 1985, *ApJ*, 290, 108
- Young, J. S., & Scoville, N. 1982, *ApJ*, 258, 467
- . 1991, *ARA&A*, 29, 581
- Zinnecker, H., et al. 2002, in *IAU Symp. 207, Extragalactic Star Clusters*, ed. D. Geisler, E. K. Grebel, & D. Minniti (San Francisco: ASP), 531